

OKINAWA INSTITUTE OF SCIENCE AND TECHNOLOGY  
GRADUATE UNIVERSITY

Thesis submitted for the degree

Doctor of Philosophy

---

**Mathematical Modeling and  
Numerical Analysis of Unstretchable  
Elastic Ribbons**

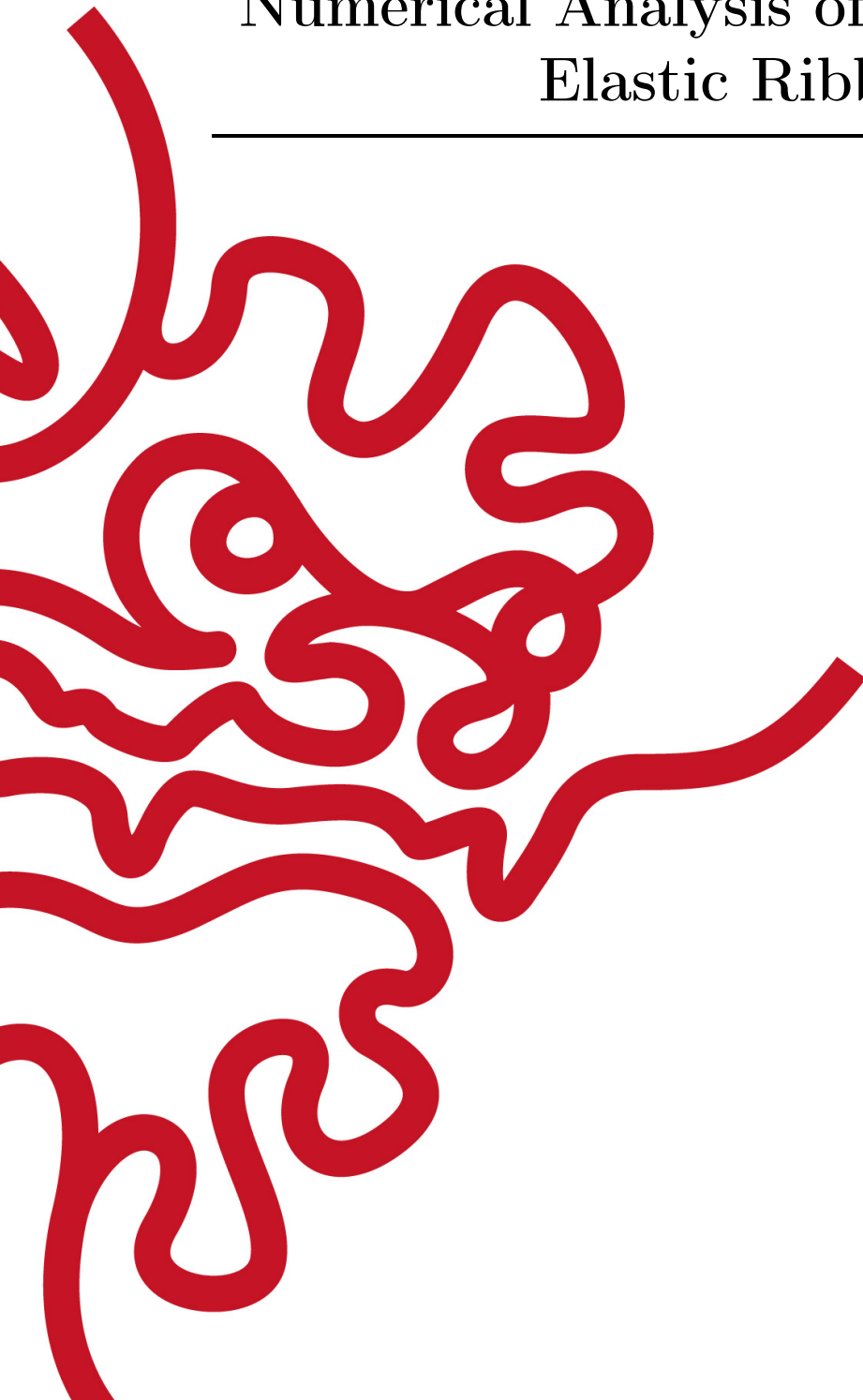
---

by

**Dmitrii Koldaev**

Supervisor: **Eliot Fried**

August 2022





# Declaration of Original and Sole Authorship

I, Dmitrii Koldaev, declare that this thesis entitled *Mathematical Modeling and Numerical Analysis of Unstretchable Elastic Ribbons* and the data presented in it are original and my own work.

I confirm that:

- No part of this work has previously been submitted for a degree at this or any other university.
- References to the work of others have been clearly acknowledged. Quotations from the work of others have been clearly indicated, and attributed to them.
- In cases where others have contributed to part of this work, such contribution has been clearly acknowledged and distinguished from my own work.
- None of this work has been previously published elsewhere.

Date: August 2022

Dmitrii Koldaev

A handwritten signature in black ink, consisting of a stylized 'M' followed by 'kg'.



# Abstract

Being able to model stable states of elastic ribbons can be beneficial for understanding various natural phenomena in physics, biology and chemistry. Ribbons also find their application in engineering. However, identifying stable state of an unstretchable elastic ribbon is a hard task. When modeling a material that bends easily but cannot extend or contract much without tearing or creasing as a two-dimensional elastic body, its resistance to elongation and contraction can be incorporated considering only deformations under which the distances between material points are preserved. The primary objective of this thesis is to develop numerical methods for finding stable equilibria of an unstretchable two-dimensional elastic material bent so that its short edges are joined, with or without twist, to form a closed band. For certain parametrizations of the reference and deformed surfaces, a dimension reduction converts the problem to one involving a system of ordinary differential equations for a pair of vector fields satisfying certain constraints that derive from the requirement that the material be unstretchable and periodicity or antiperiodicity conditions that incorporate the way in which the short edges of the strip are joined. We discretize this problem to obtain a multi-dimensional constrained optimization problem that is solved numerically. To incorporate the discrete isometry constraints, we use Lagrange multipliers approach and minimize an accordingly augmented version of the bending energy. Additionally, we introduce an alternative constraint to ensure that the deformation is injective. The new constraint is bilateral and obviates the need to impose inequality constraints, removes a certain singular feature of the energy density and circumvents symmetry assumptions that have been imposed in all previous studies of this kind.



# Acknowledgment

I am sincerely thankful to Johannes Schönke, who originally proposed a constructive representation of the discrete formulation for unstretchable elastic bands, for always supporting me during my Ph.D. program and proofreading this manuscript. Without his advice on numerical methods and their implementation, this thesis would not be possible.



# Contents

<b>Declaration of Original and Sole Authorship</b>	<b>iii</b>
<b>Abstract</b>	<b>v</b>
<b>Acknowledgment</b>	<b>vii</b>
<b>Contents</b>	<b>ix</b>
<b>List of Figures</b>	<b>xi</b>
<b>Introduction</b>	<b>1</b>
<b>1 Continuous model</b>	<b>5</b>
1.1 Right-circular cylindrical reference domain . . . . .	6
1.2 Dimensional reduction of the dimensionless bending energy functional .	10
1.3 Bilateral constraint for injectivity . . . . .	12
1.4 Equilibrium equations . . . . .	13
<b>2 Numerical approach</b>	<b>17</b>
2.1 Discretization of the optimization problem . . . . .	17
2.1.1 Constructive meaning of each of the discrete constraints . . . .	19
2.2 Convergence of the discrete functional to the continuous functional . .	22
2.3 Saddle-free Newton method . . . . .	25
2.3.1 Unconstrained optimization . . . . .	26
2.3.2 Constrained optimization . . . . .	27
<b>3 Numerical results</b>	<b>29</b>
3.1 Numerical strategies . . . . .	29
3.2 Cylindrical band . . . . .	30
3.2.1 Initial guess . . . . .	30
3.2.2 Results and analysis . . . . .	32
3.3 $\pi$ -twisted Möbius band . . . . .	34
3.3.1 Initial guess . . . . .	34
3.3.2 Results and analysis . . . . .	38
3.4 $3\pi$ -twisted Möbius band . . . . .	38

---

3.4.1	Initial guess . . . . .	38
3.4.2	Results and analysis . . . . .	38
3.5	Implications on the stability of the continuous solution . . . . .	40
3.6	Energy convergence for $\pi$ -twisted bands . . . . .	42
<b>Conclusion</b>		<b>45</b>
<b>Bibliography</b>		<b>47</b>

# List of Figures

1	Cylindrical ring and the partially everted cylinder that was obtained by deforming the cylindrical ring. . . . .	2
2.1	Flat rectangular strip constructed from vector $\mathbf{m}_i$ , $i \in \{1, \dots, N\}$ and $\mathbf{g}_i$ , $i \in \{1, \dots, N + 1\}$ . . . . .	19
2.2	Rotating one trapezoid relative to an adjacent one around common ruling.	21
3.1	Auxiliary incremental process to obtain the initial guess for a partially everted cylinder for $K = 25$ (see (3.8)) and number of flat segments $N = 20$ . The generators $\mathbf{g}_1$ and $\mathbf{g}_{11}$ are marked green. The figure on the left corresponds to $k = 0$ (discrete cylindrical ring); in the center, $k = 13$ ; on the and in right, $k = 25$ . . . . .	31
3.2	Auxiliary process of rotating half of the band to obtain initial guess for the partially everted cylinder for $K = 25$ and $N = 20$ . The generators $\mathbf{g}_1$ and $\mathbf{g}_{21}$ are marked green. . . . .	31
3.3	Geometric properties of the discrete partially everted cylinder for $b = 0.03$ .	32
3.4	Lagrange multipliers of the discrete partially everted cylinder for $b = 0.03$ .	33
3.5	The shape of the partially everted cylinder for $N = 160$ and $b = 0.03$ . Only half of the generators are shown in the picture. . . . .	34
3.6	The process of constructing an initial guess for a $\pi$ -twisted Möbius band from a cylindrical ring. . . . .	35
3.7	Examples of $\pi$ -twisted Möbius bands of width $b = 0.3$ (left) and almost maximum width $b = 1.5$ (right). Both of the bands are converged minima of the optimization problem (2.19). . . . .	35
3.8	Geometric properties of the $\pi$ -twisted Möbius bands. . . . .	36
3.9	Lagrange multipliers of the $\pi$ -twisted Möbius bands. . . . .	37
3.10	Initial guess from Schönke <i>et al.</i> [1] . . . . .	39
3.11	Examples of $3\pi$ -twisted Möbius band of width $b = 0.3$ (left) and almost maximum width $b = 0.65$ (right). . . . .	39
3.12	Geometric properties of the $3\pi$ -twisted Möbius bands. . . . .	40
3.13	Lagrange multipliers of the $3\pi$ -twisted Möbius bands. . . . .	41
3.14	Sorted and equally distributed on $[0, 1]$ eigenvalues of the projected Hessian in a logarithmic scale. The left plot corresponds to a cylindrical band of length $\ell = 2\pi$ and half-width $b = 0.3$ , and the right plot corresponds to a $\pi$ -twisted Möbius band of length $\ell = 2\pi$ and half-width $b = 0.5$ . . . . .	42

- 3.15 Möbius band made of a paper strip and a partially everted Möbius band  
obtained from it by an isometric deformation. . . . . 46

# Introduction

We can find ribbons in various phenomena in nature. Koens and Lauga [2] while studying ribbons behaviour in viscous fluid, provide a good overview of examples of ribbons in nature. They discuss examples both in flora [3] and fauna [4, 5] as well as on the microscopic level of life [6]. Additionally, the shape of classical Möbius band obtained from a strip by twisting and connecting its short edges is of interest because of the diverse range of applications. Some single crystals can be formed in the shape of Möbius band [7]. The eigenstates of a particle confined to Möbius topology were found to have some curvature effects [8] and a superconducting Möbius band positioned in a magnetic field were predicted to produce new states. Thus, algorithms for finding equilibrium states of Möbius bands as well as other ribbons have practical interest.

The classical theory of ribbons, developed by Sadowsky and Wunderlich, has recently received renewed attention. Around a hundred years ago, Sadowsky [9, 10] mathematically posed a problem of finding equilibrium shapes of an unstretchable elastic Möbius band. In this work, he derived a bending energy functional for the special case when the strip has infinitesimal width. Later Wunderlich [11, 12] derived the bending energy functional for all band widths. In 2007 Starostin and van der Heijden [13, 14] published studies where they provide a shape of unstretchable elastic Möbius band. However, there are significant limitations in their approach. First, the authors do not explicitly consider the deformation and thus it is unclear if the isometry constraint (the surface distance between any two material points is preserved under the deformation) is properly taken care of. Second, only symmetric solutions are considered *a priori*. Also, no analysis is done on the stability of the obtained equilibria. However, for any practical application only stable configurations are of interest as only those will keep their shape. In 2016 Moore and Healey [15] presented approach of an equilibrium configuration for the complete unsupported Möbius strip and assessing the stability of flip-symmetric configurations. Only symmetric variations are considered for the stability analysis. Additionally, only very limited range of narrow bands are studied due to numerical challenges. A rigorous treatment of unstretchable elastic material surfaces has been developed by Chen, Fosdick and Fried [16], where for the first time equilibrium conditions were derived using variational principles. These equilibrium conditions are derived without approximation and represent boundary-value problems for finding the shape of the surface, a symmetric second-order tensor-valued Lagrange multiplier field (which admits a representation as a symmetric  $2 \times 2$  matrix), and a scalar-valued Lagrange multiplier field. A dimensionally reduced optimization problem for finding equilibrium shapes based on ruled parametrization of the reference and deformed surfaces is derived by Seguin *et al.* [17]. In this study, we provide a

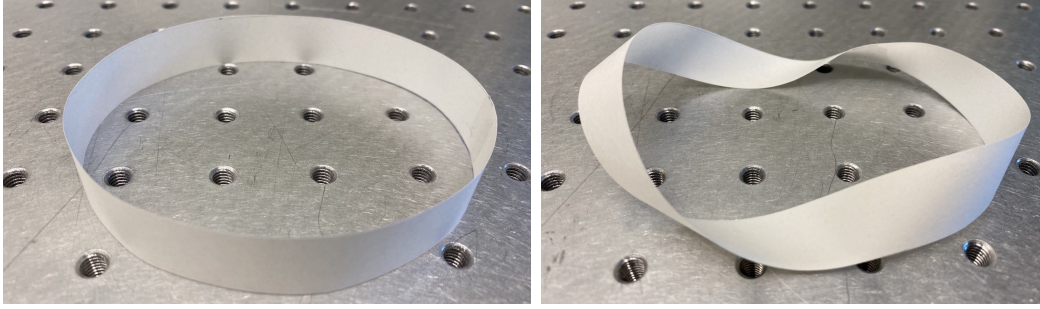


**Figure 1:** Cylindrical ring and the partially everted cylinder that was obtained by deforming the cylindrical ring.

modification to this optimization problem that removes the singularities of the energy functional and makes the development of numerical approaches more straightforward.

Another motivation for this thesis is that there are configurations for elastic bands that have never been studied in the literature. For example, a right-circular cylindrical ring (left in Figure 1) is a global minimum for an unstretchable elastic band with circular topology. However, there is another supposedly stable configuration for bands with cylindrical topology that can be obtained from a cylindrical band made of paper. We call this configuration a partially everted cylinder (right in Figure 1). As we are interested in studying the deformation from a right-circular cylindrical ring to the partially everted cylinder, we chose the reference configuration to be the right-circular cylindrical shape. This allows us to avoid the change of topology and the necessity to deal with gluing conditions that are unavoidable consequences of working with a rectangular reference configuration. However, the results present in Section 1.3 can be also applied, with slight modification, to the optimization problem with rectangular strip reference configuration as in Seguin *et al.* [17].

In Chapter 1, we derive the continuous optimization problem. We require that any point in space can be occupied by at most one material point. Thus, we consider an injective isometric deformation  $\chi$  of a two-dimensional homogeneous and isotropic solid identified with a right-circular cylindrical reference configuration  $\mathcal{D}$  into a band that occupies the surface  $\mathcal{S}$  in three-dimensional Euclidean point space. We assume that no loads are applied neither to the surface  $\mathcal{S}$  itself, nor to the edge  $\partial\mathcal{S}$  of  $\mathcal{S}$ . Following Sadowsky [9, 10], we assume that the energy stored, per unit area, in deforming  $\mathcal{D}$  to  $\mathcal{S}$  is proportional to the square of the mean curvature  $H$  of  $\mathcal{S}$ . To obtain the equilibria of unstretchable elastic bands, we thus seek solutions of the problem

$$\min_{\chi} \int_{\mathcal{S}} H^2 ds \quad \text{subject to} \quad (\nabla\chi)^T \nabla\chi = \mathbf{I}_{\mathcal{D}},$$

where  $\mathbf{I}_{\mathcal{D}}$  is the (surface) identity tensor on  $\mathcal{D}$ .

One of the fundamental requirements for the deformation  $\chi$  is that it must be injective. As it is hard to globally ensure the injectivity, Starostin and van der Heijden [13, 14], Moore and Healey [15], Seguin *et al.* [17] introduce a local injectivity constraint that is acceptable as long as there is no self-contact of the surface. However, the need to fulfill this constraint makes numerical implementation more complicated.

One problem is that the local injectivity constraint used in these works is unilateral and requires special treatment such as the active set method [18]. But more importantly, when the constraint is active, the energy density is hard to compute numerically as it contains an unbounded multiplier. Previously, Starostin and van der Heijden [13] and Moore and Healey [15] assumed symmetry of the solution that helped them to stabilize the numerics. However, this assumption is a significant limitation, as there is no proof that the solution must be symmetric, and for the stability analysis, it is not enough to consider only symmetric variations. In this study, we suggest an alternative bilateral constraint that allows us to rewrite the energy functional in a more numerically stable form. It is important to notice that the change excludes the possibility of the injectivity constraint (1.50) to be active. As discussed in Seguin *et. al.* [17], if the injectivity constraint is active on some interval, the corresponding portion of the deformed surface must be flat. Thus, excluding the possibility of the injectivity constraint to be active infers the *a priori* assumption that the deformed surface has no flat portions. However, it is valid to make this assumption due to the results of Hornung [19] where he proves that the deformed surface must have no flat region.

In Chapter 2, we discretize the continuous problem for obtaining equilibrium shapes of unstretchable elastic ribbons and thus obtain a corresponding discrete optimization problem. We also show how to reconstruct a continuous surface given a solution to the discrete problem. Additionally, we establish the connection between folding a rectangular strip and the discrete isometry constraints. Another issue that is addressed in this study is the search for a local minimum in the discrete case. One of the difficulties in solving high-dimensional optimization problem is the proliferation of saddle points. The standard Newton method tends to be attracted to saddle points and the gradient descent method, which is not attracted to saddle points, has problems with scaling of the step. A saddle-free Newton's approach for unconstrained optimization was proposed in Dauphin et al [20]. We generalize the saddle-free approach for the case of constrained optimization with equality constraints and successfully apply this approach.

In Chapter 3, we provide numerical solutions to the discrete optimization problem obtained in Chapter 2 for bands with circular,  $\pi$ -twisted Möbius and  $3\pi$ -twisted Möbius topology. As we have explicitly introduce all of the isometry constraints and use the Lagrange multipliers approach to incorporate them, we also obtain the reaction forces corresponding to the constraints. We also have a good quantitative agreement with the results by Starostin and van der Heijden [13], [14] and Moore and Healey [15]. At the same time, we were able to obtain the  $3\pi$ -twisted Möbius band for a wider range of half-width to length aspect ratios. Our numerical results support the assumption previously made by Starostin and van der Heijden [13, 14] and Moore and Healey [15] that the minimizers for  $\pi$ -twisted and  $3\pi$ -twisted bands have certain symmetries. However, in this study we did not assume any symmetry *a priori* and the symmetry is an *a posteriori* result. Finally, to make sure that the obtained configurations are minimizers, we tested all of the discrete solutions using the second order condition of the projected Hessian defined in Section 2.3.



# Chapter 1

## Continuous model

In this chapter, we focus on presenting the derivation of a one-dimensional optimization problem for finding equilibria of unstretchable elastic bands. We consider an injective isometric deformation of a two-dimensional homogeneous and isotropic solid identified with a right-circular cylindrical reference configuration  $\mathcal{D}$  of circumference  $\ell$  and half-width  $b$  into a band that occupies the surface  $\mathcal{S}$  in three-dimensional Euclidean point space. Let  $\mathbf{x}$  denote a material point belonging to  $\mathcal{D}$  and let  $\boldsymbol{\chi}$  be a smooth isometric deformation from  $\mathcal{D}$  to the surface  $\mathcal{S}$ . A material point  $\mathbf{x}$  of the reference surface  $\mathcal{D}$  is thus mapped to

$$\mathbf{r} = \boldsymbol{\chi}(\mathbf{x}) \quad (1.1)$$

under the deformation  $\boldsymbol{\chi}$ . The requirement that the deformation be isometric is equivalent to the requirement that the metric tensor on  $\mathcal{S}$  being identical  $(\nabla\boldsymbol{\chi})^T\nabla\boldsymbol{\chi} = \mathbf{I}_{\mathcal{D}}$  on  $\mathcal{D}$ , where  $\mathbf{I}_{\mathcal{D}}$  is the (surface) identity tensor on  $\mathcal{D}$ . We assume that no loads are applied neither to the surface  $\mathcal{S}$  itself, nor to the edge  $\partial\mathcal{S}$  of  $\mathcal{S}$ . To obtain the equilibria of unstretchable elastic bands, we thus seek solutions of the problem

$$\min_{\boldsymbol{\chi}} \int_{\mathcal{S}} H^2 ds \quad \text{subject to} \quad (\nabla\boldsymbol{\chi})^T\nabla\boldsymbol{\chi} = \mathbf{I}_{\mathcal{D}}. \quad (1.2)$$

In previous works by Sadowsky [10], Wunderlich [11], Mahadevan and Keller [21], Starostin and van der Heijden [13], Hornung [19], Moore and Healey [15] and Seguin *et al.* [17], the reference configuration has been taken to be a rectangular strip. As the main result of this chapter, we derive the dimensionally reduced optimization problem for the untwisted band with the reference configuration being right-circular cylindrical. This novel choice allows us to avoid the change of topology and the necessity to deal with gluing conditions that are unavoidable consequences of working with a rectangular reference configuration. We also show that the choice of reference configuration adopted here leads to an optimization problem that is essentially identical to that formulated by Seguin *et al.* [17]. However, the optimization problem formulated in Seguin *et al.* [17] is derived for the wider class of bands with arbitrary number of twists. As in the work of Seguin *et al.* [17], the deformed surface is here parametrized as a ruled surface. However, the generatrix is normalized differently. It is possible to use this normalization to describe the deformation of an unstretchable, homogeneous, isotropic material surface from a rectangular reference configuration, and thus, with reference

to Seguin *et al.* [17], we later use the optimization problem obtained in this chapter for twisted bands. However, it is important to keep the choice of reference configuration in mind when interpreting the results for twisted bands. Another result of this chapter is a bilateral constraint for local injectivity of the deformation. It becomes possible to write the optimization problem without inequality constraints by introducing this constraint and also remove certain singularities from the energy density as we show in Section 1.3. We conclude the chapter by deriving the Euler-Lagrange equations and explicitly computing the Lagrange multipliers that were used to incorporate the isometry and the new bilateral injectivity constraint.

## 1.1 Right-circular cylindrical reference domain

Consider the parameter set

$$\mathcal{P} = [0, \ell) \times (-b, b) \quad (1.3)$$

and two functions  $\widehat{\mathbf{x}} : \mathcal{P} \rightarrow \mathcal{D}$  and  $\widehat{\mathbf{r}} : \mathcal{P} \rightarrow \mathcal{S}$  that parametrize material points on the reference and deformed surfaces  $\mathcal{D}$  and  $\mathcal{S}$ , respectively. We omit regularity assumptions and simply assume that  $\widehat{\mathbf{x}}$  and  $\widehat{\mathbf{r}}$  are as smooth as needed to ensure the existence of any derivatives that may appear. We choose functions  $\widehat{\mathbf{x}}$  and  $\widehat{\mathbf{r}}$  that admit the following representations on  $\mathcal{P}$

$$\mathbf{x} = \widehat{\mathbf{x}}(\alpha, \beta) = \mathbf{c}(\alpha) + \mathbf{f}(\alpha, \beta), \quad (1.4)$$

$$\mathbf{r} = \widehat{\mathbf{r}}(\alpha, \beta) = \mathbf{d}(\alpha) + \beta \mathbf{g}(\alpha), \quad (1.5)$$

where:

- $\mathbf{r}(\mathbf{x})$  denotes the material point of  $\mathcal{S}$  corresponding to the material point  $\mathbf{x}$  of  $\mathcal{D}$ , so that

$$\mathbf{r}(\mathbf{c}(\alpha) + \mathbf{f}(\alpha, \beta)) = \mathbf{d}(\alpha) + \beta \mathbf{g}(\alpha) \quad (1.6)$$

for each parameter pair  $(\alpha, \beta) \in \mathcal{P}$ ;

- $\mathbf{c}(\alpha)$  - parametrizes the midline of the reference cylindrical shape and  $\mathbf{f}(\alpha, \beta)$  is some function that we derive later from the requirement that the deformation must be isometric;
- the directrix  $\mathbf{d}$  and generatrix  $\mathbf{g}$  must satisfy the periodicity conditions

$$\lim_{\alpha \rightarrow \ell} \mathbf{d}(\alpha) = \mathbf{d}(0), \quad \lim_{\alpha \rightarrow \ell} \mathbf{g}(\alpha) = \mathbf{g}(0), \quad \lim_{\alpha \rightarrow \ell} \mathbf{d}_{,\alpha}(\alpha) = \mathbf{d}_{,\alpha}(0), \quad (1.7)$$

and the condition that ensure that the mapping from  $\mathcal{P}$  to  $\mathcal{S}$  is locally injective

$$1 + \beta \mathbf{d}_{,\alpha}(\alpha) \cdot \mathbf{g}_{,\alpha}(\beta) > 0, \quad (\alpha, \beta) \in \mathcal{P}, \quad (1.8)$$

where dot denotes scalar product and a subscript preceded by a comma denotes differentiation with respect to the subscripted quantity (eg  $\mathbf{d}_{,\alpha} = \frac{d\mathbf{d}}{d\alpha}$ , we later use same notation for the derivatives with respect to  $\beta$ ). Note that here and after repeated indices do not mean summation;

- the normalization condition for the representation of the surface in the reference configuration is

$$|\mathbf{c}_{,\alpha}| = 1; \quad (1.9)$$

- the normalization conditions for the representation of the surface in the deformed configuration are

$$|\mathbf{d}_{,\alpha}| = 1 \quad \text{and} \quad |\mathbf{g}|^2 = (\mathbf{g} \cdot \mathbf{d}_{,\alpha})^2 + 1, \quad (1.10)$$

- closure constraint for the deformed surface

$$\mathbf{d}(0) = \mathbf{d}(\ell), \quad \mathbf{g}(0) = \mathbf{g}(\ell) \quad \text{and} \quad (\mathbf{d}_{,\alpha} \cdot \mathbf{g})(0) = (\mathbf{d}_{,\alpha} \cdot \mathbf{g})(\ell). \quad (1.11)$$

In contrast to the condition (1.6) which establishes a one-to-one correspondence between material points on the reference and deformed surfaces and thus defines the deformation  $\chi$ , conditions (1.9) and (1.10) are ancillary. However, these conditions facilitate the derivation of the optimization problem in terms of the deformed surface and the subsequent dimensional reduction. The normalizations of  $\mathbf{c}$  and  $\mathbf{d}$  can differ from those chosen in (1.9) and (1.10), but they need to be consistent with each other. The normalization of the generatrix  $\mathbf{g}$  in (1.10) can also be different. For example, in Seguin *et al.* [17], the authors choose the generatrix to be of unit length. Different normalizations generally lead to a different parameter set  $\mathcal{P}$  and different forms of the energy density and the isometry constraints. The normalization used in this study was chosen because of the relatively concise form of the energy functional that ensues on its basis.

For the deformation  $\chi$  from  $\mathcal{D}$  to  $\mathcal{S}$  to be isometric, it is necessary to impose restrictions on the deformation gradient that were originally derived by Chen *et al.* [22]. Those authors consider the inverse of the one-to-one correspondence between points on the reference surface and points in the parameters set induced by the parametrization of the reference surface (1.4). This leads to two scalar mappings  $\tilde{\alpha}$  and  $\tilde{\beta}$  defined on the reference surface  $\mathcal{D}$ . In the dual basis induced by these two scalar mappings, the requirement that the metric tensor be preserved under the deformation  $\chi$  leads to the following restrictions on the corresponding parametrizations  $\hat{\mathbf{x}}$  and  $\hat{\mathbf{r}}$ :

$$\hat{\mathbf{x}}_{,\alpha} \cdot \hat{\mathbf{x}}_{,\alpha} = \hat{\mathbf{r}}_{,\alpha} \cdot \hat{\mathbf{r}}_{,\alpha}, \quad (1.12)$$

$$\hat{\mathbf{x}}_{,\beta} \cdot \hat{\mathbf{x}}_{,\beta} = \hat{\mathbf{r}}_{,\beta} \cdot \hat{\mathbf{r}}_{,\beta}, \quad (1.13)$$

$$\hat{\mathbf{x}}_{,\alpha} \cdot \hat{\mathbf{x}}_{,\beta} = \hat{\mathbf{r}}_{,\alpha} \cdot \hat{\mathbf{r}}_{,\beta}. \quad (1.14)$$

Using (1.4) and (1.5) in (1.12)–(1.14) leads to three scalar constraints:

$$2\mathbf{c}_{,\alpha} \cdot \mathbf{f}_{,\alpha} + \mathbf{f}_{,\alpha} \cdot \mathbf{f}_{,\alpha} = 2\beta \mathbf{d}_{,\alpha} \cdot \mathbf{g}_{,\alpha} + \beta^2 |\mathbf{g}_{,\alpha}|^2, \quad (1.15)$$

$$\mathbf{f}_{,\beta} \cdot \mathbf{f}_{,\beta} = \mathbf{g} \cdot \mathbf{g} = (\mathbf{g} \cdot \mathbf{d}_{,\alpha})^2 + 1, \quad (1.16)$$

$$(\mathbf{c}_{,\alpha} + \mathbf{f}_{,\alpha}) \cdot \mathbf{f}_{,\beta} = \mathbf{d}_{,\alpha} \cdot \mathbf{g} + \beta \mathbf{g}_{,\alpha} \cdot \mathbf{g}. \quad (1.17)$$

We next establish isometry constraints analogous to (80) of Seguin *et al.* [17]. Moreover, we demonstrate that those constraints lead to the isometry conditions (1.15)–

(1.17). Let  $\{\mathbf{v}_1, \mathbf{v}_2, \mathbf{v}_3\}$  denote a positively oriented basis in three-dimensional Euclidean vector space. The midline of the referential cylinder  $\mathcal{D}$  can then be parametrized as

$$\mathbf{c}(\alpha) = R \cos\left(\frac{\alpha}{R}\right) \mathbf{v}_1 + R \sin\left(\frac{\alpha}{R}\right) \mathbf{v}_2, \quad \alpha \in [0, l), \quad (1.18)$$

where  $R = l/2\pi$ . As the ruling through the point  $\mathbf{d}(\alpha_0)$  associated with an arbitrary fixed  $\alpha_0 \in [0, l)$  is a geodesic on  $\mathcal{S}$ , the curve  $\widehat{\mathbf{x}}(\alpha_0, \beta)$ ,  $\beta \in [0, b]$  must be a geodesic on  $\mathcal{D}$ . The only non-trivial (non-planar) geodesics on a cylinder passing through the midline are circular helices. Using the isometry condition (1.16), we arrive at the following representation of  $\widehat{\mathbf{x}}(\alpha, \beta)$  in the form of a helix

$$\widehat{\mathbf{x}}(\alpha, \beta) = R \cos\left(\frac{(\mathbf{d}_{,\alpha}(\alpha) \cdot \mathbf{g}(\alpha))\beta + \alpha}{R}\right) \mathbf{v}_1 + R \sin\left(\frac{(\mathbf{d}_{,\alpha}(\alpha) \cdot \mathbf{g}(\alpha))\beta + \alpha}{R}\right) \mathbf{v}_2 + \beta \mathbf{v}_3, \quad (1.19)$$

where  $(\alpha, \beta) \in \mathcal{P} = [0, \ell) \times [-b, b]$ . Differentiating (1.15) with respect to  $\beta$  and (1.17) with respect to  $\alpha$ , we obtain

$$\mathbf{d}_{,\alpha\alpha} \cdot \mathbf{g} = (\mathbf{c}_{,\alpha\alpha} + \mathbf{f}_{,\alpha\alpha}) \cdot \mathbf{f}_{,\beta} - (\mathbf{g}_{,\alpha\alpha} \cdot \mathbf{g})_{,\beta} = \widehat{\mathbf{x}}_{,\alpha\alpha} \cdot \widehat{\mathbf{x}}_{,\beta} - (\mathbf{g}_{,\alpha\alpha} \cdot \mathbf{g})_{,\beta} \quad (1.20)$$

Using the form of the helices (1.19) and computing the derivatives of  $\widehat{\mathbf{x}}$ , we arrive at the condition

$$\widehat{\mathbf{x}}_{,\alpha\alpha} \cdot \widehat{\mathbf{x}}_{,\beta} = (\mathbf{d}_{,\alpha} \cdot \mathbf{g})_{,\alpha\alpha} \cdot (\mathbf{d}_{,\alpha} \cdot \mathbf{g})_{,\beta}. \quad (1.21)$$

Now we compute  $\widehat{\mathbf{x}}_{,\alpha} \cdot \widehat{\mathbf{x}}_{,\alpha}$  using (1.19) and use (1.15), giving

$$|\mathbf{g}_{,\alpha}|^2 = [(\mathbf{d}_{,\alpha} \cdot \mathbf{g})_{,\alpha}]^2. \quad (1.22)$$

Computing the second derivatives of the center and left-hand side of (1.16), we find that

$$\mathbf{g} \cdot \mathbf{g}_{,\alpha\alpha} + |\mathbf{g}_{,\alpha}|^2 = (\mathbf{d}_{,\alpha} \cdot \mathbf{g})_{,\alpha\alpha} \cdot (\mathbf{d}_{,\alpha} \cdot \mathbf{g}) + [(\mathbf{d}_{,\alpha} \cdot \mathbf{g})_{,\alpha}]^2. \quad (1.23)$$

Using (1.22), (1.23) and then (1.20) and (1.21), we obtain the condition

$$\mathbf{d}_{,\alpha\alpha} \cdot \mathbf{g} = 0. \quad (1.24)$$

Next we introduce the Darboux frame  $\{\mathbf{t}, \mathbf{n}, \mathbf{b}\}$  for the midline of  $\mathcal{S}$  via

$$\mathbf{t} = \mathbf{d}_{,\alpha}, \quad \mathbf{n} = \mathbf{g} \times \mathbf{t}, \quad \mathbf{b} = \mathbf{t} \times \mathbf{n}. \quad (1.25)$$

It can then be shown that

$$\begin{aligned} \mathbf{t}_{,\alpha} &= \kappa_n \mathbf{n} + \kappa_g \mathbf{b}, \\ \mathbf{n}_{,\alpha} &= -\kappa_n \mathbf{t} + \tau_g \mathbf{b}, \\ \mathbf{b}_{,\alpha} &= -\kappa_g \mathbf{t} - \tau_n \mathbf{n}, \end{aligned}$$

where  $\kappa_n$  and  $\kappa_g$  are the normal and geodesic curvatures of the midline of  $\mathcal{S}$  and  $\tau_g$  is the corresponding geodesic torsion. Granted that the midline parameterized by  $\mathbf{c}$  is a geodesic on the referential cylinder  $\mathcal{D}$  and that the deformation from  $\mathcal{D}$  to  $\mathcal{S}$  is

isometric, the derivatives of elements of the Darboux frame simplify to the following relations

$$\mathbf{t}_\alpha = \kappa \mathbf{n}, \quad (1.26)$$

$$\mathbf{n}_\alpha = -\kappa \mathbf{t} + \tau \mathbf{b}, \quad (1.27)$$

$$\mathbf{b}_\alpha = -\tau \mathbf{n}, \quad (1.28)$$

where  $\kappa = \kappa_n$  (as  $\kappa_g = 0$ ) and  $\tau = \tau_g$  respectively denote the curvature and torsion of the directrix parameterized by  $\mathbf{d}$ . In this basis, the generatrix has the decomposition

$$\mathbf{g} = (\mathbf{g} \cdot \mathbf{t})\mathbf{t} + \mathbf{b}. \quad (1.29)$$

Next, we compute the derivative of  $\mathbf{g}$  and its magnitude and invoke (1.28) to find that

$$\mathbf{g}_{,\alpha} = (\mathbf{g} \cdot \mathbf{t})_\alpha \mathbf{t} + (\mathbf{g} \cdot \mathbf{t})\kappa \mathbf{n} - \tau \mathbf{n}, \quad (1.30)$$

$$|\mathbf{g}_\alpha|^2 = [(\mathbf{g} \cdot \mathbf{t})_\alpha]^2 + [(\mathbf{g} \cdot \mathbf{t})\kappa - \tau]^2. \quad (1.31)$$

By comparing (1.31) with (1.22), we conclude that

$$(\mathbf{g} \cdot \mathbf{t})\kappa - \tau = 0. \quad (1.32)$$

Thus, we obtain an additional isometry condition of the form

$$(\mathbf{t} \times \mathbf{g}) \cdot \mathbf{g}_\alpha = -(\mathbf{g} \cdot \mathbf{t})[(\mathbf{g} \cdot \mathbf{t})\kappa - \tau] = 0. \quad (1.33)$$

In summary, we have the following normalization and necessary isometry conditions:

$$|\mathbf{d}_{,\alpha}| = 1, \quad |\mathbf{g}|^2 = (\mathbf{g} \cdot \mathbf{d}_{,\alpha})^2 + 1, \quad \mathbf{d}_{,\alpha\alpha} \cdot \mathbf{g} = 0, \quad (\mathbf{d}_{,\alpha} \times \mathbf{g}) \cdot \mathbf{g}_\alpha = 0. \quad (1.34)$$

The next step is to ensure that the conditions in (1.34) are sufficient to ensure that the deformation  $\boldsymbol{\chi}$  from the referential cylinder  $\mathcal{D}$  to the surface  $\mathcal{S}$  is isometric. First, by directly computing the scalar product, we can see that the referential normalization (1.9) follows from the representation of the midline (1.18). The validity of (1.16) can be established by differentiating (1.19) with respect to  $\beta$  and computing the scalar product of the obtained derivative with itself. Similarly, (1.17) is the result of computing  $\widehat{\mathbf{x}}_\alpha$  and  $\widehat{\mathbf{x}}_\beta$  and then taking their scalar product and invoking (1.34)<sub>2</sub> to give

$$\widehat{\mathbf{x}}_\alpha \cdot \widehat{\mathbf{x}}_\beta = (\mathbf{d}_{,\alpha} \cdot \mathbf{g}) + \beta (\mathbf{d}_{,\alpha} \cdot \mathbf{g})_\alpha (\mathbf{d}_{,\alpha} \cdot \mathbf{g}) = (\mathbf{d}_{,\alpha} \cdot \mathbf{g}) + \beta (\mathbf{g} \cdot \mathbf{g}_\alpha). \quad (1.35)$$

To obtain (1.15), consider the scalar product

$$\widehat{\mathbf{x}}_\alpha \cdot \widehat{\mathbf{x}}_\alpha = 1 + 2\beta (\mathbf{d}_{,\alpha} \cdot \mathbf{g})_\alpha + \beta^2 [(\mathbf{d}_{,\alpha} \cdot \mathbf{g})_\alpha]^2. \quad (1.36)$$

Using (1.34)<sub>3</sub>, we see that  $(\mathbf{d}_{,\alpha} \cdot \mathbf{g})_\alpha = \mathbf{d}_{,\alpha} \cdot \mathbf{g}_\alpha$  and it thus only remains to show that  $[(\mathbf{d}_{,\alpha} \cdot \mathbf{g})_\alpha]^2 = |\mathbf{g}_\alpha|^2$ . It follows from (1.34)<sub>4</sub> that  $\mathbf{g}_\alpha$  can be decomposed into a linear combination of  $\mathbf{g}$  and  $\mathbf{d}_{,\alpha}$ :

$$\mathbf{g}_\alpha = \xi \mathbf{g} + \theta \mathbf{d}_{,\alpha}. \quad (1.37)$$

Multiplying (1.37) by  $\mathbf{g}$  and  $\mathbf{d}_{,\alpha}$  and employing (1.34)<sub>2</sub> and (1.34)<sub>3</sub>, we find that  $\xi = 0$  and that  $\theta = \mathbf{g}_\alpha \cdot \mathbf{d}_{,\alpha}$ . Thus, we conclude that

$$\mathbf{g}_\alpha \cdot \mathbf{g}_\alpha = (\mathbf{g}_\alpha \cdot \mathbf{d}_{,\alpha})^2 = (\mathbf{g}_\alpha \cdot \mathbf{d}_{,\alpha} + \mathbf{d}_{,\alpha\alpha} \cdot \mathbf{g})^2 = [(\mathbf{d}_{,\alpha} \cdot \mathbf{g})_\alpha]^2. \quad (1.38)$$

This fact finishes the proof that (1.34) are not only necessary but also sufficient conditions for  $\widehat{\mathbf{r}}$  of a form (1.5) to parametrize the image  $\mathcal{S}$  of an isometric deformation of the reference cylinder  $\mathcal{D}$ . Let us now formulate the above as a theorem.

**Theorem.** The region  $\mathcal{S}$  with representation (1.5) occupied by the deformed material cylinder is an image of an isometric deformation  $\chi = \widehat{\mathbf{r}} \circ \widehat{\mathbf{x}}^{-1}$  of the reference configuration  $\mathcal{D}$  with representation (1.4) occupied by reference right-circular cylindrical surface of radius  $\ell/2\pi$  and altitude  $2b$  if and only if the directrix  $\mathbf{d}$  and generatrix  $\mathbf{g}$  satisfy

$$\mathbf{d}_{,\alpha\alpha} \cdot \mathbf{g} = 0 \quad \text{and} \quad (\mathbf{d}_{,\alpha} \times \mathbf{g}) \cdot \mathbf{g}_\alpha = 0 \quad (1.39)$$

on their common domain of definition  $[0, \ell)$ .

## 1.2 Dimensional reduction of the dimensionless bending energy functional

We assume that  $\mathcal{D}$  was formed by bending, without stretching a homogeneous and isotropic two-dimensional material rectangle of length  $\ell$  and halfwidth  $b$ .<sup>1</sup> In this sense,  $\mathcal{D}$  has no spontaneous curvature. Thus, any open subset  $\mathcal{A}$  of  $\mathcal{D}$  that might be excised from  $\mathcal{D}$  would spontaneously open onto a planar region without changing the distance between any two material points of  $\mathcal{A}$ . In particular, severing  $\mathcal{D}$  along one of its generators will produce a rectangular material strip of length  $\ell$  and half-width  $b$  while preserving the distance between any two material points of  $\mathcal{D}$ . It consequently follows that the energy stored, per unit area, in an isometric deformation  $\chi$  of  $\mathcal{D}$  to a configuration  $\mathcal{S}$  depends only on the mean curvature  $H$  of  $\mathcal{S}$ . We assume for simplicity that the stored energy density to be a quadratic function of  $H$ , in which case the total dimensionless bending energy  $E$  of  $\mathcal{S}$  is given by

$$E = \int_{\mathcal{S}} H^2 da, \quad (1.40)$$

where  $da$  is the area element of  $\mathcal{S}$ . We next show that (1.40) reduces to a line integral over the midline  $\mathcal{C}$  of  $\mathcal{S}$ .

Let  $\eta = \mathbf{t} \cdot \mathbf{g} = \mathbf{d}_{,\alpha} \cdot \mathbf{g}$ . We can then use (1.29) to rewrite the representation (1.5) of the deformed surface  $\mathcal{S}$  in the form

$$\widehat{\mathbf{r}}(\alpha, \beta) = \mathbf{d} + \beta (\eta \mathbf{t} + \mathbf{b}). \quad (1.41)$$

---

<sup>1</sup>The material rectangle from which  $\mathcal{D}$  is formed should not be conflated with the set  $\mathcal{P} = [0, \ell) \times [-b, b]$  of ordered parameter pairs  $(\alpha, \beta)$  used in defining the parametrizations  $\widehat{\mathbf{x}}$  and  $\widehat{\mathbf{r}}$  of the reference and spatial configurations  $\mathcal{D}$  and  $\mathcal{S}$ .

## 1.2 Dimensional reduction of the dimensionless bending energy functional

From the derivatives

$$\widehat{\mathbf{r}}_{,\alpha} = (1 + \beta\eta_\alpha) \mathbf{t}, \quad \widehat{\mathbf{r}}_{,\beta} = \eta \mathbf{t} + \mathbf{b}, \quad (1.42)$$

of  $\widehat{\mathbf{r}}$ , we see that the components of the first fundamental form  $\mathbf{I}$  of  $\mathcal{S}$  are given by:

$$I_{\alpha\alpha} = \widehat{\mathbf{r}}_{,\alpha} \cdot \widehat{\mathbf{r}}_{,\alpha} = (1 + \beta\eta_\alpha)^2, \quad I_{\alpha\beta} = I_{\beta\alpha} = \widehat{\mathbf{r}}_{,\alpha} \cdot \widehat{\mathbf{r}}_{,\beta} = \eta(1 + \beta\eta_\alpha), \quad I_{\beta\beta} = \widehat{\mathbf{r}}_{,\beta} \cdot \widehat{\mathbf{r}}_{,\beta} = 1 + \eta^2. \quad (1.43)$$

Next, from second derivatives

$$\widehat{\mathbf{r}}_{,\alpha\alpha} = \kappa(1 + \beta\eta_\alpha) \mathbf{n} + \beta\eta_{,\alpha\alpha} \mathbf{t}, \quad \widehat{\mathbf{r}}_{,\alpha\beta} = \eta_{,\alpha} \mathbf{t}, \quad \widehat{\mathbf{r}}_{,\beta\beta} = \mathbf{0}, \quad (1.44)$$

we arrive at the following components of the second fundamental form  $\mathbf{II}$  of  $\mathcal{S}$ :

$$II_{\alpha\alpha} = \widehat{\mathbf{r}}_{,\alpha\alpha} \cdot \mathbf{n} = \kappa(1 + \beta\eta_\alpha), \quad II_{\alpha\beta} = II_{\beta\alpha} = \widehat{\mathbf{r}}_{,\alpha\beta} \cdot \mathbf{n} = 0, \quad II_{\beta\beta} = \widehat{\mathbf{r}}_{,\beta\beta} \cdot \mathbf{n} = 0. \quad (1.45)$$

The mean curvature  $H$  and area element  $da$  of the deformed surface  $\mathcal{S}$  are thus given by

$$H = \frac{1}{2 \det I} (I_{\alpha\alpha} II_{\beta\beta} + I_{\alpha\alpha} II_{\beta\beta} - 2I_{\alpha\beta} II_{\alpha\beta}) = \frac{\kappa(1 + \eta^2)}{2(1 + \beta\eta_\alpha)}, \quad (1.46)$$

$$da = \sqrt{\det I} d\alpha d\beta = (1 + \beta\eta_\alpha) d\alpha d\beta. \quad (1.47)$$

We can now express the dimensionless bending energy functional (1.40) as

$$E = \int_0^l \int_{-b}^b \frac{\kappa^2(1 + \eta^2)^2}{4(1 + \beta\eta_\alpha)} d\beta d\alpha = \frac{1}{4} \int_0^l \frac{\kappa^2(1 + \eta^2)^2}{\eta_\alpha} \log \frac{1 + b\eta_\alpha}{1 - b\eta_\alpha} d\alpha = E_w. \quad (1.48)$$

Apart from its constant prefactor, the right-hand of (1.48) is the well-known Wunderlich [11] functional. This outcome is consistent with the assumption that the reference configuration  $\mathcal{D}$  has no spontaneous curvature and, hence, might have been anticipated. Before Wunderlich, Sadowsky [10] derived the energy functional for the special case in which  $H$  and  $da$  are approximated by choosing  $\beta = 0$  in (1.46) and (1.47), respectively.

As a consequence of (1.48), we obtain a dimensionally reduced problem for finding equilibrium shapes of unstretchable elastic untwisted bands:

$$\begin{aligned} \min_{\mathbf{d}, \mathbf{g}} E_w &= \min_{\mathbf{d}, \mathbf{g}} \frac{1}{4} \int_0^l \frac{\kappa^2(1 + \eta^2)^2}{\eta'} \log \frac{1 + b\eta'}{1 - b\eta'} d\alpha \\ &\text{subject to} \\ |\mathbf{d}'| &= 1, \quad |\mathbf{g}'|^2 = (\mathbf{d}' \cdot \mathbf{g}')^2 + 1, \quad \mathbf{d}'' \cdot \mathbf{g} = 0, \quad (\mathbf{d}' \times \mathbf{g}') \cdot \mathbf{g}' = 0, \\ &1 \pm b\eta' \geq 0, \\ \mathbf{d}(0) &= \mathbf{d}(l), \quad \mathbf{g}(0) = \mathbf{g}(l), \end{aligned} \quad (1.49)$$

where  $\kappa = |\mathbf{d}''|$  and  $\eta = \mathbf{d}' \cdot \mathbf{g}$ . As the problem (1.49) is one dimensional, we have used a prime to indicate differentiation with respect to the arclength  $\alpha$  along the directrix and will continue that practice hereinafter. In writing (1.49), we have explicitly included

the local injectivity constraint

$$1 \pm b\eta' \geq 0. \quad (1.50)$$

This constraint ensures that there is no local interpenetration of the surface. It is important to be aware that the fundamental requirement that the deformation be injective is not fully represented by this local constraint. Surfaces that exhibit self-contact are therefore beyond the scope of the present research. Also, we can see that the set of equations is the same as those provided by Seguin *et al.* [17], except for different form of the normalization constraint  $|\mathbf{g}|^2 = (\mathbf{d}' \cdot \mathbf{g})^2 + 1$  on the generatrix  $\mathbf{g}$ .

### 1.3 Bilateral constraint for injectivity

The optimization problem (1.49) involves bilateral and unilateral constraints. The unilateral injectivity constraint complicates the development of a numerical approach for solving (1.49). Moreover, when the constraint is active (that is, when equality is achieved), some multipliers in the energy density diverge, bringing another challenge to the numerical implementation. However, it is possible to reformulate the problem by adding an additional constraint that substitutes for the injectivity constraint. Upon noticing that

$$2 \operatorname{atanh} x = \log \frac{1+x}{1-x}, \quad x \in (-1, 1), \quad (1.51)$$

it is reasonable to introduce a new variable  $\xi$  that satisfies the constraint

$$\tanh \xi(\alpha) = b\eta'(\alpha), \quad \alpha \in [0, \ell]. \quad (1.52)$$

Since the image of  $\tanh$  always lies in  $(-1, 1)$ , the injectivity constraint (1.50) is automatically fulfilled. It is important to notice that (1.52) alters the solution space. In particular, it excludes the possibility of  $\eta'(\alpha) = \pm 1/b$ . If the injectivity constraint is active for some  $\alpha \in [0, \ell)$  then corresponding portion of  $\mathcal{S}$  must be flat as shown in Seguin *et al.* [17]. However, as shown by Hornung [19], local minimizers never have flat regions. Thus, substitution of the constraints is not restrictive.

Additionally, using the new constraint, we can rewrite the energy density

$$e_w(\mathbf{d}, \mathbf{g}) = \frac{1}{4} |\mathbf{d}''|^2 |\mathbf{g}|^4 \frac{1}{b \mathbf{d}' \cdot \mathbf{g}'} \log \frac{1 + b \mathbf{d}' \cdot \mathbf{g}'}{1 - b \mathbf{d}' \cdot \mathbf{g}'} \quad (1.53)$$

$$= \frac{1}{2} |\mathbf{d}''|^2 |\mathbf{g}|^4 \frac{\xi}{\tanh \xi} = q(\mathbf{d}, \mathbf{g}, \xi). \quad (1.54)$$

The motivation for rewriting the functional comes from the numerical solution perspective. The original energy density  $e_w(\mathbf{d}, \mathbf{g})$  contains the multiplier

$$\frac{1}{b \mathbf{d}' \cdot \mathbf{g}'} \log \frac{1 + b \mathbf{d}' \cdot \mathbf{g}'}{1 - b \mathbf{d}' \cdot \mathbf{g}'} \quad (1.55)$$

that diverges at all pairs of  $\mathbf{d}$  and  $\mathbf{g}$  such that  $\mathbf{d}' \cdot \mathbf{g}' = \pm 1/b$ . Even though that does not imply anything about  $e_w(\mathbf{d}, \mathbf{g})$ , the discrete counterpart of the multiplier (1.55) is hard to implement numerically. Even a small change in  $\mathbf{d}$  or  $\mathbf{g}$  can cause the multiplier

to become infinitely large and thus cause the numerical algorithm to fail. On the other hand, after the change of variables, the new integrand has the multiplier

$$\frac{\xi}{\tanh \xi} \quad (1.56)$$

that only get infinite when  $\xi$  gets infinite. The change of variables thus allows us to develop a stable numerical algorithm for finding equilibria of unstretchable elastic bands that we present in later chapters. The minimization problem (1.49) can now be recast as

$$\begin{aligned} \min_{\mathbf{d}, \mathbf{g}, \xi} Q &= \min_{\mathbf{d}, \mathbf{g}, \xi} \frac{b}{2} \int_0^l |\mathbf{d}''|^2 |\mathbf{g}|^4 \frac{\xi}{\tanh \xi} d\alpha, \\ &\text{subject to} \\ |\mathbf{d}'|^2 &= 1, \quad |\mathbf{g}|^2 = (\mathbf{d}' \cdot \mathbf{g})^2 + 1, \quad \mathbf{d}'' \cdot \mathbf{g} = 0, \quad (\mathbf{d}' \times \mathbf{g}) \cdot \mathbf{g}' = 0, \quad b \mathbf{d}' \cdot \mathbf{g}' = \tanh \xi, \\ &\mathbf{d}(0) = \mathbf{d}(l), \quad \mathbf{g}(0) = \mathbf{g}(l). \end{aligned} \quad (1.57)$$

We finally introduce Lagrange multipliers  $\lambda_1(\alpha)$ ,  $\lambda_2(\alpha)$ ,  $\lambda_3(\alpha)$ ,  $\lambda_4(\alpha)$ ,  $\lambda_5(\alpha)$ . These are not merely convenient tools to find equilibria, but also represent reaction forces associated with the corresponding constraints. Using Lagrange multipliers, we can write the new augmented energy function

$$\begin{aligned} E_a[\mathbf{d}, \mathbf{g}, \xi] &= \int_0^l \left[ \frac{b}{2} |\mathbf{d}''|^2 |\mathbf{g}|^4 \frac{\xi}{\tanh \xi} - \lambda_1 (|\mathbf{d}'|^2 - 1) - \lambda_2 (|\mathbf{g}|^2 - \eta^2 - 1) \right. \\ &\quad \left. - \lambda_3 (\mathbf{d}'' \cdot \mathbf{g}) - \lambda_4 (\mathbf{d}' \times \mathbf{g}) \cdot \mathbf{g}' - \lambda_5 (b \mathbf{d}' \cdot \mathbf{g}' - \tanh \xi) \right] d\alpha - \gamma \cdot \int_0^l \mathbf{d}' d\alpha. \end{aligned} \quad (1.58)$$

As we are interested in studying reaction forces in the bands, it is important to introduce the continuous Lagrange multipliers. This allows us to formulate the discrete optimization problem in Chapter 2 in a way that the corresponding discrete Lagrange multipliers approximate the continuous counterparts.

## 1.4 Equilibrium equations

To obtain a weak statement of the conditions that must hold in equilibrium, we set the first variation of the augmented energy (1.58)

$$\begin{aligned} \delta E_a[\mathbf{d}, \mathbf{g}, \xi] &= \int_0^l \left[ \zeta_{\mathbf{g}} \cdot \delta \mathbf{g} + \zeta_{\xi} \delta \xi + \zeta_{\mathbf{d}''} \cdot \delta \mathbf{d}'' \right. \\ &\quad - 2\lambda_1 \mathbf{d}' \cdot \delta \mathbf{d}' - 2\lambda_2 (\mathbf{g} \cdot \delta \mathbf{g} - (\mathbf{d}' \cdot \mathbf{g})(\mathbf{d}' \cdot \delta \mathbf{g} + \mathbf{g} \cdot \delta \mathbf{d}')) \\ &\quad - \lambda_3 (\mathbf{d}'' \cdot \delta \mathbf{g} + \mathbf{g} \cdot \delta \mathbf{d}'') - \lambda_4 ((\mathbf{g} \times \mathbf{g}') \cdot \delta \mathbf{d}' - (\mathbf{d}' \times \mathbf{g}) \cdot \delta \mathbf{g}') \\ &\quad \left. - \lambda_5 (b \mathbf{d}' \cdot \delta \mathbf{g}' + b \mathbf{g}' \cdot \delta \mathbf{d}' - (\tanh \xi)_{\xi} \delta \xi) \right] d\alpha \end{aligned} \quad (1.59)$$

equal to zero. In the variation above we used the notation

$$\zeta(\mathbf{g}, \xi, \mathbf{d}'') = \frac{b}{2} |\mathbf{d}''|^2 |\mathbf{g}|^4 \frac{\xi}{\tanh \xi}. \quad (1.60)$$

In (1.59) we used the fact that  $\mathbf{d}'$  is collinear with  $\mathbf{g}'$  to eliminate the term with  $\mathbf{d}' \times \mathbf{g}'$ . For convenience, the variation can be rewritten in the form

$$\delta E[\mathbf{d}, \mathbf{g}, \xi] = \int_0^\ell \left[ \boldsymbol{\sigma}_{\mathbf{d}''} \cdot \delta \mathbf{d}'' + \boldsymbol{\sigma}_{\mathbf{d}'} \cdot \delta \mathbf{d}' + \boldsymbol{\sigma}_{\mathbf{g}'} \cdot \delta \mathbf{g}' + \boldsymbol{\sigma}_{\mathbf{g}} \cdot \delta \mathbf{g} + \sigma_\xi \delta \xi \right] d\alpha$$

using the following notations

$$\begin{aligned} \boldsymbol{\sigma}_{\mathbf{d}''} &= \zeta_{\mathbf{d}''} - \lambda_3 \mathbf{g}, \\ \boldsymbol{\sigma}_{\mathbf{d}'} &= -2\lambda_1 \mathbf{d}' + 2\lambda_2 (\mathbf{d}' \cdot \mathbf{g}) \mathbf{g} - \lambda_4 (\mathbf{g} \times \mathbf{g}') - b\lambda_5 \mathbf{g}', \\ \boldsymbol{\sigma}_{\mathbf{g}'} &= -\lambda_4 (\mathbf{d}' \times \mathbf{g}) - b\lambda_5 \mathbf{d}', \\ \boldsymbol{\sigma}_{\mathbf{g}} &= \zeta_{\mathbf{g}} - 2\lambda_2 (\mathbf{g} - (\mathbf{d}' \cdot \mathbf{g}) \mathbf{d}') - \lambda_3 \mathbf{d}'', \\ \sigma_\xi &= \zeta_\xi + \lambda_5 (\tanh \xi)_\xi. \end{aligned}$$

After integration by parts, we arrive at

$$\begin{aligned} \delta E[\mathbf{d}, \mathbf{g}, \xi] &= \int_0^\ell \left[ (\boldsymbol{\sigma}_{\mathbf{d}''}' - \boldsymbol{\sigma}_{\mathbf{d}'}') \cdot \delta \mathbf{d} + (-\boldsymbol{\sigma}_{\mathbf{g}'}' + \boldsymbol{\sigma}_{\mathbf{g}}) \cdot \delta \mathbf{g} + \sigma_\xi \delta \xi \right] d\alpha \\ &\quad + \left( \boldsymbol{\sigma}_{\mathbf{d}''} \cdot \delta \mathbf{d}' + (-\boldsymbol{\sigma}_{\mathbf{d}''}' + \boldsymbol{\sigma}_{\mathbf{d}'}) \cdot \delta \mathbf{d} + \boldsymbol{\sigma}_{\mathbf{g}'} \cdot \delta \mathbf{g} \right) \Big|_0^\ell. \end{aligned}$$

From the requirement that the first variation  $\delta E[\mathbf{d}, \mathbf{g}, \xi]$  must vanish for all admissible variations  $\delta \mathbf{d}$ ,  $\delta \mathbf{g}$  and  $\delta \xi$ , we obtain Euler–Lagrange equations

$$(\zeta_{\mathbf{d}''} - \lambda_3 \mathbf{g})'' + (2\lambda_1 \mathbf{d}' - 2\lambda_2 (\mathbf{d}' \cdot \mathbf{g}) \mathbf{g} + \lambda_4 (\mathbf{g} \times \mathbf{g}') + b\lambda_5 \mathbf{g}')' = \mathbf{0}, \quad (1.61)$$

$$(\lambda_4 (\mathbf{d}' \times \mathbf{g}) + b\lambda_5 \mathbf{d}')' + \zeta_{\mathbf{g}} - 2\lambda_2 (\mathbf{g} - (\mathbf{d}' \cdot \mathbf{g}) \mathbf{d}') - \lambda_3 \mathbf{d}'' = \mathbf{0}, \quad (1.62)$$

$$\zeta_\xi + \lambda_5 \xi \operatorname{sech}^2 \xi = 0, \quad (1.63)$$

that need to be fulfilled for all  $\alpha \in (0, \ell)$  and the matching boundary conditions

$$(\zeta_{\mathbf{d}''} - \lambda_3 \mathbf{g})(0) = (\zeta_{\mathbf{d}''} - \lambda_3 \mathbf{g})(\ell), \quad (1.64)$$

$$\begin{aligned} &((\zeta_{\mathbf{d}''} - \lambda_3 \mathbf{g})' - 2\lambda_1 \mathbf{d}' - 2\lambda_2 (\mathbf{d}' \cdot \mathbf{g}) \mathbf{g} - \lambda_4 (\mathbf{g} \times \mathbf{g}') - b\lambda_5 \mathbf{g}')(0) = \\ &((\zeta_{\mathbf{d}''} - \lambda_3 \mathbf{g})' - 2\lambda_1 \mathbf{d}' - 2\lambda_2 (\mathbf{d}' \cdot \mathbf{g}) \mathbf{g} - \lambda_4 (\mathbf{g} \times \mathbf{g}') - b\lambda_5 \mathbf{g}')(\ell), \end{aligned} \quad (1.65)$$

$$\begin{aligned} &(\zeta_{\mathbf{g}} - 2\lambda_2 (\mathbf{g} - (\mathbf{d}' \cdot \mathbf{g}) \mathbf{d}') - \lambda_3 \mathbf{d}'')(0) = \\ &(\zeta_{\mathbf{g}} - 2\lambda_2 (\mathbf{g} - (\mathbf{d}' \cdot \mathbf{g}) \mathbf{d}') - \lambda_3 \mathbf{d}'')(\ell). \end{aligned} \quad (1.66)$$

From the isometry equation  $\mathbf{d}'' \cdot \mathbf{g} = 0$ , we can see that the boundary condition (1.64) is equivalent to the two requirements

$$\zeta_{\mathbf{d}''}(0) = \zeta_{\mathbf{d}''}(\ell) \quad \text{and} \quad (\lambda_3 \mathbf{g})(0) = (\lambda_3 \mathbf{g})(\ell). \quad (1.67)$$

Additionally, using the isometry equation  $|\mathbf{d}'| = 1$ , from (1.66) we imply

$$(\zeta_{\mathbf{g}} - \lambda_2(\mathbf{g} - (\mathbf{d}' \cdot \mathbf{g})\mathbf{d}'))(0) = (\zeta_{\mathbf{g}} - \lambda_2(\mathbf{g} - (\mathbf{d}' \cdot \mathbf{g})\mathbf{d}'))(\ell), \quad (1.68)$$

$$(\lambda_3 \mathbf{d}'')(0) = (\lambda_3 \mathbf{d}'')(\ell). \quad (1.69)$$

Another useful property of the new formulation using additional variable  $\xi$  is that the Lagrange multipliers can be obtained explicitly in terms of  $\mathbf{d}$ ,  $\mathbf{g}$  and  $\xi$ . From (1.63) we immediately obtain

$$\lambda_5 = -\frac{\zeta_{\xi}}{\xi \operatorname{sech}^2 \xi}. \quad (1.70)$$

We expand the derivative in (1.62) to get

$$\dot{\lambda}_4(\mathbf{d}' \times \mathbf{g}) + \lambda_4(\mathbf{d}'' \times \mathbf{g}) + b\dot{\lambda}_5 \mathbf{d}' + b\lambda_5 \mathbf{d}'' + \zeta_{\mathbf{g}} - 2\lambda_2(\mathbf{g} - (\mathbf{d}' \cdot \mathbf{g})\mathbf{d}') - \lambda_3 \mathbf{d}'' = \mathbf{0}. \quad (1.71)$$

Next we multiply (1.62) by  $\mathbf{g}$ ,  $\mathbf{d}'$  and  $\mathbf{d}''$  and get the equations that can be resolved for  $\lambda_2$ ,  $\lambda_3$ ,  $\lambda_4$ :

$$b\dot{\lambda}_5 \mathbf{d}' \cdot \mathbf{g} - 2\lambda_2 = -\zeta_{\mathbf{g}} \cdot \mathbf{g}, \quad (1.72)$$

$$\lambda_4(\mathbf{d}'' \times \mathbf{g}) \cdot \mathbf{d}' + b\dot{\lambda}_5 = -\zeta_{\mathbf{g}} \cdot \mathbf{d}', \quad (1.73)$$

$$\dot{\lambda}_4(\mathbf{d}' \times \mathbf{g}) \cdot \mathbf{d}'' + (b\lambda_5 - \lambda_3)|\mathbf{d}''|^2 = -\zeta_{\mathbf{g}} \cdot \mathbf{d}''. \quad (1.74)$$

The Lagrange multipliers  $\lambda_2$ ,  $\lambda_3$ ,  $\lambda_4$  then take the form

$$\lambda_2 = \frac{1}{2}(\zeta_{\mathbf{g}} \cdot \mathbf{g} - b(\zeta_{\xi}/(\xi \operatorname{sech}^2 \xi))' \mathbf{d}' \cdot \mathbf{g}), \quad (1.75)$$

$$\lambda_4 = \frac{b\zeta_{\xi}/(\xi \operatorname{sech}^2 \xi)' - \zeta_{\mathbf{g}} \cdot \mathbf{d}'}{(\mathbf{d}'' \times \mathbf{g}) \cdot \mathbf{d}'}, \quad (1.76)$$

$$\lambda_3 = \frac{\dot{\lambda}_4(\mathbf{d}' \times \mathbf{g}) \cdot \mathbf{d}''}{|\mathbf{d}''|^2} + b\lambda_5, \quad (1.77)$$

where we used the special Wunderlich functional form to eliminate  $\zeta_{\mathbf{g}} \cdot \mathbf{d}''$ . Finally, we can also obtain  $\lambda_1$  from (1.61).

$$\lambda_1 = \frac{1}{2}((\zeta_{\mathbf{d}} - \lambda_3 \mathbf{g})'' \cdot \mathbf{d}' - (2\lambda_2(\mathbf{d}' \cdot \mathbf{g})^2 + b\lambda_5 \mathbf{g}' \cdot \mathbf{d}' + \boldsymbol{\gamma} \cdot \mathbf{d}')), \quad (1.78)$$

where  $\boldsymbol{\gamma}$  is a constant three dimensional vector obtained from the integration of (1.61). It can also be viewed as the reaction force that keep the band closed.



# Chapter 2

## Numerical approach

In the previous chapter, we obtained a one-dimensional optimization problem for finding equilibrium shapes of free standing ribbons that are topologically equivalent to a cylindrical ring of radius  $\ell/2\pi$  and height  $2b$ . Using the results obtained in Seguin *et al.* [17] for a wider class of bands, we can generalize the problem to the bands with twisted topologies and knotless midlines. The change in the optimization problem will only appear in the condition  $\mathbf{g}(0) = \mathbf{g}(\ell)$  that should be replaced by

$$\mathbf{g}(0) = \mathbf{g}(\ell) \quad \text{if the band is orientable,} \quad (2.1)$$

$$\mathbf{g}(0) = -\mathbf{g}(\ell) \quad \text{otherwise.} \quad (2.2)$$

However, even this dimensionally reduced problem is hard to tackle analytically. In this chapter we obtain a discretized version of the continuous optimization problem (1.57). We show that the corresponding discrete augmented energy functional approximates the continuous counterpart (1.58) to second order in the step-size used to represent the directrix as a discrete chain of straight lines of equal length. We also present a saddle-free Newton-type optimization method for tackling the discrete optimization problem.

### 2.1 Discretization of the optimization problem

Let the interval  $[0, \ell]$  be represented by  $N$  subintervals  $I_i = (\alpha_i, \alpha_{i+1}]$ ,  $i \in \{1, \dots, N\}$ , with  $0 = \alpha_1 < \dots < \alpha_{N+1} = \ell$  and  $\alpha_{i+1} = \alpha_i + h$ , where  $h = \ell/N$ . Vectorial quantities  $\mathbf{d}_i$  and  $\mathbf{g}_i$  are defined at integer nodes  $i$ ,  $i \in \{1, n+1\}$  by the rules

$$\mathbf{d}_i = \mathbf{d}(\alpha_i) \quad \text{and} \quad \mathbf{g}_i = \mathbf{g}(\alpha_i). \quad (2.3)$$

We also introduce

$$\mathbf{u} = \mathbf{d}' \quad (2.4)$$

and approximate it, along with  $\xi$ , at half-nodes  $\alpha_{i+1/2} = \alpha_i + h/2$  by the rules

$$\mathbf{u}_i = \mathbf{u}(\alpha_{i+1/2}) \quad \text{and} \quad \xi_i = \xi(\alpha_{i+1/2}), \quad i \in \{1, \dots, N\}. \quad (2.5)$$

On using the foregoing notational conventions, we discretize the isometry and injectivity constraints of the problem (1.57) at  $\alpha_i$  or  $\alpha_{i+1/2}$ , giving

$$(|\mathbf{d}'|^2 - 1)(\alpha_{i+1/2}) = |\mathbf{u}_i|^2 - 1, \quad (2.6)$$

$$(|\mathbf{g}|^2 - (\mathbf{d}' \cdot \mathbf{g})^2 - 1)(\alpha_i) = |\mathbf{g}_i|^2 - \left( \frac{\mathbf{u}_i + \mathbf{u}_{i-1}}{2} \cdot \mathbf{g}_i \right)^2 - 1, \quad (2.7)$$

$$((\mathbf{d}' \times \mathbf{g}) \cdot \mathbf{g}')(\alpha_{i+1/2}) \approx \left( \mathbf{u}_i \times \frac{\mathbf{g}_{i+1} + \mathbf{g}_i}{2} \right) \cdot \left( \frac{\mathbf{g}_{i+1} - \mathbf{g}_i}{h} \right), \quad (2.8)$$

$$\mathbf{d}'' \cdot \mathbf{g}(\alpha_i) \approx \frac{\mathbf{u}_i - \mathbf{u}_{i-1}}{h} \cdot \mathbf{g}_i = 0, \quad (2.9)$$

$$(w\mathbf{u} \cdot \mathbf{g}' - \tanh \xi)(\alpha_{i+1/2}) \approx w\mathbf{u}_i \cdot \frac{\mathbf{g}_{i+1} - \mathbf{g}_i}{h} - \tanh \xi_i, \quad (2.10)$$

where  $i \in \{1, \dots, N\}$ . The constraints are then approximated by requiring that the right-hand sides of (2.6)–(2.10) vanish. Explanations for these approximations are provided in the next subsection.

The energy  $Q$  from (1.57) can now be discretized in the following way:

$$Q = \sum_{i=1}^N \frac{b}{2} \int_{\alpha_{i-1/2}}^{\alpha_{i+1/2}} |\mathbf{d}''|^2 |\mathbf{g}|^4 \frac{\xi}{\tanh \xi} d\alpha \quad (2.11)$$

$$= \sum_{i=1}^N \frac{b}{2} \int_{\alpha_{i-1/2}}^{\alpha_{i+1/2}} |\mathbf{u}'(\alpha_i)|^2 |\mathbf{g}(\alpha_i)|^4 \frac{\xi(\alpha_i)}{\tanh \xi(\alpha_i)} d\alpha \quad (2.12)$$

$$\approx b \sum_{i=1}^N \left| \frac{\mathbf{u}_{i+1} - \mathbf{u}_i}{h} \right|^2 |\mathbf{g}_i|^4 \frac{(\xi_i + \xi_{i-1})/2}{\tanh((\xi_i + \xi_{i-1})/2)} h \quad (2.13)$$

$$= \sum_{i=1}^N q_i \rho_i^4 a_i / h = Q_h, \quad (2.14)$$

where  $q_i$ ,  $\rho_i$ , and  $a_i$  are defined for each  $i \in \{0, n\}$  by

$$q_i = 1 - \mathbf{u}_i \cdot \mathbf{u}_{i-1}, \quad \rho_i^4 = |\mathbf{g}_i|^4, \quad \text{and} \quad a_i = b \frac{(\xi_i + \xi_{i-1})/2}{\tanh((\xi_i + \xi_{i-1})/2)}. \quad (2.15)$$

To obtain (2.15)<sub>1</sub>, we used the discrete midline normalization constraint (2.6)

$$q_i = |\mathbf{u}_i - \mathbf{u}_{i-1}|^2 = |\mathbf{u}_i|^2 - 2\mathbf{u}_i \cdot \mathbf{u}_{i-1} + |\mathbf{u}_{i-1}|^2 = 2(1 - \mathbf{u}_i \cdot \mathbf{u}_{i-1}). \quad (2.16)$$

We also discretize the constraint (1.11)<sub>1</sub> that closes the midline, giving

$$\int_0^l \mathbf{d}' d\alpha \approx \sum_{i=1}^N \mathbf{u}_i h = 0. \quad (2.17)$$

Using the constraint (2.8) to simplify (2.7), we arrive at the set of the isometry con-

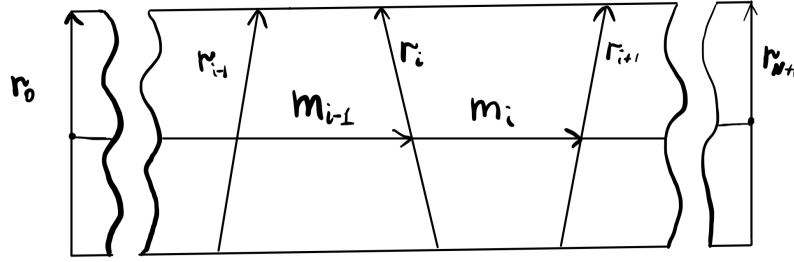


**Figure 2.1:** Flat rectangular strip constructed from vector  $\mathbf{m}_i$ ,  $i \in \{1, \dots, N\}$  and  $\mathbf{g}_i$ ,  $i \in \{1, \dots, N + 1\}$ .

straints

$$|\mathbf{u}_i| = 1, \quad |\mathbf{g}_i|^2 = (\mathbf{g}_i \cdot \mathbf{u}_i)^2 + 1, \quad (\mathbf{u}_i - \mathbf{u}_{i-1}) \cdot \mathbf{g}_i = 0, \quad (\mathbf{u}_i \times \mathbf{g}_i) \cdot \mathbf{g}_{i+1} = 0. \quad (2.18)$$

Finally, the problem of finding minima of the discrete functional  $Q_h$  derived in (2.13) subject to the isometry (2.6)–(2.9), injectivity (2.10), and closure constraints (2.2), (2.17) can be written in the following form

$$\min_{\mathbf{u}_i, \mathbf{g}_i, \xi_i, i \in \{1, \dots, N\}} E_D = \min_{\mathbf{u}_i, \mathbf{g}_i, \xi_i, i \in \{1, \dots, N\}} \sum_{i=1}^N \frac{q_i \rho_i^4 a_i}{h}$$

subject to

$$|\mathbf{u}_i| = 1, \quad |\mathbf{g}_i|^2 = (\mathbf{g}_i \cdot \mathbf{u}_i)^2 + 1, \quad (\mathbf{u}_i - \mathbf{u}_{i-1}) \cdot \mathbf{g}_i = 0, \quad (\mathbf{u}_i \times \mathbf{g}_i) \cdot \mathbf{g}_{i+1} = 0, \quad (2.19)$$

$$\frac{w}{h} \mathbf{u}_i \cdot \mathbf{g}_{i+1} - \mathbf{g}_i - \tanh \xi_i = 0,$$

$$\sum_{j=0}^N \mathbf{u}_j = 0, \quad \mathbf{g}_1 = \pm \mathbf{g}_{N+1},$$

where  $i = 1, \dots, N$ ,  $q_i$ ,  $\rho_i$ ,  $a_i$  are as defined in (2.15), and the sign on the left-hand side of the last equation is fixed by the orientability of the band.

### 2.1.1 Constructive meaning of each of the discrete constraints

In (2.6)–(2.10), we discretized some constraints at nodes  $\alpha_i$  and others at half-nodes  $\alpha_{i+1/2}$ . There is a discrete surface that can be represented by this set of discrete isometry constraints. This surface is a chain of flat segments of trapezoidal or triangular shape. On the other hand, the same set of geometric constraints can be obtained for a surface that is obtained from a rectangular strip folded  $N$  times along rulings that pass through the midline. Thus, when establishing a connection between the discrete and continuous formulations, we also establish a connection between the folding of a rectangular strip and its isometric bending.

Consider a flat rectangular strip of length  $\ell$  and width  $2b$  divided into  $N$  quadrilaterals. The upper parts of the  $N$  flat segments are obtained from  $N$  midline elements

$\mathbf{m}_i, i \in \{1, \dots, N\}$  and  $N + 1$  rulings  $\mathbf{r}_i$  as shown in Figure 2.1. We constrain the rulings  $\mathbf{r}_i$  and  $\mathbf{r}_{i+1}$  to emanate from the initial and terminal points, respectively, of the midline element  $\mathbf{m}_i$  to the edge of the strip. The lower parts of the quadrilaterals are obtained from  $-\mathbf{r}_i$  and  $-\mathbf{r}_{i+1}$ . The requirements mentioned above can be written as the set of normalization constraints for  $i \in \{1, \dots, N\}$ , which read

$$|\mathbf{m}_i| = h, \quad |\mathbf{r}_i|^2 = \left(\mathbf{r}_i \cdot \frac{\mathbf{m}_i}{h}\right)^2 + b^2, \quad 1 \pm b \frac{\mathbf{m}}{h} \cdot (\mathbf{r}_{i+1} - \mathbf{r}_i) > 0, \quad (2.20)$$

where  $h = \ell/N$ . While the first condition in (2.20) ensures that the midline segments are of uniform size, the second condition in (2.20) ensures that the rulings extend to the edges of the strip, and the last condition in (2.20) makes sure that two rulings do not meet with the reference strip and its boundary.

Let  $\tilde{\mathbf{m}}_i$  be the image of  $\mathbf{m}_i$  after folding for  $i \in \{1, \dots, N\}$  and  $\tilde{\mathbf{r}}_i$  be the image of  $\mathbf{r}_i$   $i \in \{1, \dots, N + 1\}$ . After folding, the new set of midline elements will form a chain of quadrilaterals in three dimensional Euclidean space. The spacial quadrilaterals (except in the degenerate triangular case) should be of the same shape and size as their corresponding reference quadrilaterals. If this is the case, the material points on the reference and deformed surface can be matched by aligning the quadrilaterals to which the points belong. To ensure that the spatial quadrilaterals are of the same size as their reference counterparts, it is enough to ensure that the length of the midline segments and rulings is preserved in conjunction with ensuring that  $\tilde{\mathbf{m}}_i, \tilde{\mathbf{r}}_i$  and  $\tilde{\mathbf{r}}_{i+1}$ , and the angle between  $\mathbf{m}_i$  and  $\mathbf{r}_i$  is preserved. If the three vectors  $\tilde{\mathbf{m}}_i, \tilde{\mathbf{r}}_i$  and  $\tilde{\mathbf{r}}_{i+1}$  lie in the same plane, then the following condition must hold

$$(\tilde{\mathbf{m}}_i \times \tilde{\mathbf{r}}_i) \cdot \tilde{\mathbf{r}}_{i+1} = 0, \quad i \in \{1, \dots, N\}. \quad (2.21)$$

Then the normalization conditions for the deformed surface read as

$$|\tilde{\mathbf{m}}_i| = h, \quad |\tilde{\mathbf{r}}_i|^2 = \left(\mathbf{r}_i \cdot \frac{\mathbf{m}_i}{h}\right)^2 + b^2, \quad 1 \pm b \frac{\tilde{\mathbf{m}}}{h} \cdot (\tilde{\mathbf{r}}_{i+1} - \tilde{\mathbf{r}}_i) > 0, \quad i \in \{1, \dots, N\}. \quad (2.22)$$

Finally, we need to preserve the angle between  $\mathbf{m}_i$  and  $\mathbf{r}_i$ , for  $i \in \{1, \dots, N\}$ . Consider two flat quadrilateral formed by  $\mathbf{m}_{i-1}, \mathbf{r}_{i-1}$  and  $\mathbf{r}_i$  and  $\mathbf{m}_i, \mathbf{r}_i$  and  $\mathbf{r}_{i+1}$ , respectively (shown in Figure 2.2). Without loss of generality, consider folding of one flat element relative to the other where the first flat element coincides with its reference quadrilateral after folding as shown in Figure 2.2. As the angles between  $\mathbf{m}_i$  and  $\mathbf{r}_i$  are in range  $(0, \pi)$  and the magnitudes are already preserved, it is enough to preserve the scalar product to preserve the angles, namely

$$\tilde{\mathbf{r}}_i \cdot \tilde{\mathbf{m}}_i = \mathbf{r}_i \cdot \mathbf{m}_i, \quad i \in \{1, \dots, N\}. \quad (2.23)$$

As all of the midline segments are collinear in the reference surface and the quadrilateral containing  $\mathbf{m}_{i-1}$  stays at the same position as in Figure 2.2, we can see that

$$\mathbf{r}_i \cdot \mathbf{m}_i = \mathbf{r}_i \cdot \mathbf{m}_{i-1} = \tilde{\mathbf{r}}_i \cdot \tilde{\mathbf{m}}_{i-1}, \quad i \in \{1, \dots, N\}. \quad (2.24)$$

Comparing (2.23) and (2.24), we obtain the condition for the angle between  $\mathbf{m}_i$  and  $\mathbf{r}_i$

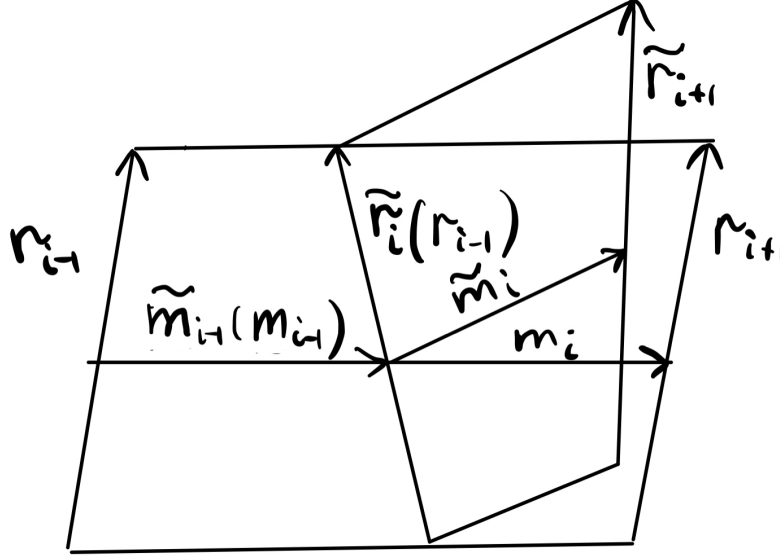


**Figure 2.2:** Rotating one trapezoid relative to an adjacent one around common ruling.

be preserved in terms  $\tilde{\mathbf{m}}_i$  and  $\tilde{\mathbf{r}}_i$

$$(\tilde{\mathbf{m}}_i - \tilde{\mathbf{m}}_{i-1}) \cdot \tilde{\mathbf{r}}_i = 0, \quad i \in \{1, \dots, N\}. \quad (2.25)$$

We can now write the isometry constraints in terms of only  $\tilde{\mathbf{m}}_i$  and  $\tilde{\mathbf{r}}_i$ , namely

$$|\tilde{\mathbf{m}}_i| = h, \quad |\tilde{\mathbf{r}}_i|^2 = \left(\tilde{\mathbf{r}}_i \cdot \frac{\tilde{\mathbf{m}}_i}{h}\right)^2 + b^2, \quad (\tilde{\mathbf{m}}_i - \tilde{\mathbf{m}}_{i-1}) \cdot \tilde{\mathbf{r}}_i = 0, \quad (\tilde{\mathbf{m}}_i \times \tilde{\mathbf{r}}_i) \cdot \tilde{\mathbf{r}}_{i+1} = 0, \quad (2.26)$$

where  $i \in \{1, \dots, N\}$ . Let us now introduce dimensionless counterparts of  $\tilde{\mathbf{m}}_i$  and  $\tilde{\mathbf{r}}_i$

$$\tilde{\mathbf{u}}_i = \frac{\tilde{\mathbf{m}}_i}{h} \quad \text{and} \quad \tilde{\mathbf{g}}_i = \frac{\tilde{\mathbf{r}}_i}{b}, \quad i \in \{1, \dots, N\}. \quad (2.27)$$

In terms of dimensionless variables  $\tilde{\mathbf{m}}_i$  and  $\tilde{\mathbf{r}}_i$ , the folding geometrical constraints take a form

$$|\tilde{\mathbf{u}}_i| = h, \quad |\tilde{\mathbf{g}}_i|^2 = (\tilde{\mathbf{g}}_i \cdot \tilde{\mathbf{u}}_i)^2 + 1, \quad (\tilde{\mathbf{u}}_i - \tilde{\mathbf{u}}_{i-1}) \cdot \tilde{\mathbf{g}}_i = 0, \quad (\tilde{\mathbf{u}}_i \times \tilde{\mathbf{g}}_i) \cdot \tilde{\mathbf{g}}_{i+1} = 0, \quad (2.28)$$

where  $i \in \{1, \dots, N\}$ , identical to the constraints (2.18) that we obtained by discretizing the continuous isometry constraints. Thus, pure bending of a strip without stretching can be associated with infinitely refined folding along the rulings emanation from the midline. However, the rulings are not known a priori and must be determined as part of the solution of any particular problem.

## 2.2 Convergence of the discrete functional to the continuous functional

In this section, we present results that complement those presented in section 2.1. Specifically, we provide a way of constructing the continuous surface from a discrete surface that satisfies all of the discrete isometry constraints. Moreover, we show that the constructed continuous surface satisfies the continuous constraints up to the second-order in the step-size  $h$  at corresponding nodes or half nodes. We also show that the difference between the continuous energy of the constructed surface and the discrete energy of the discrete surface is quadratic in  $h$ . Thus, if the Lagrange multipliers  $\lambda_i$ ,  $i = 1, \dots, N$  are properly reconstructed, the difference between the discrete and continuous Lagrangians is also quadratic in  $h$ .

Suppose that

$$\mathbf{u}_i, \quad i \in \{1, \dots, N\}, \quad (2.29)$$

$$\mathbf{g}_j, \quad j \in \{1, \dots, N + 1\}, \quad (2.30)$$

satisfy the constraints of the discrete optimization problem (2.19). Let us now construct a surface  $\mathcal{S}_c$  parametrized by  $(\alpha, \beta) \in [0, l] \times [-b, b]$  with the following properties. First, its parametrization is ruled, meaning that

$$\mathbf{r} = \tilde{\mathbf{r}}(\alpha, \beta) = \int_0^\alpha \mathbf{d}'(\hat{\alpha}) d\hat{\alpha} + \beta \mathbf{g}(\alpha), \quad (2.31)$$

where  $\mathbf{r}$  is a material point on  $\mathcal{S}_c$ . Moreover,

$$\mathbf{d}'(\alpha_{i+1/2}) = \mathbf{u}_{i+1}, \quad i \in \{0, \dots, N - 1\}, \quad (2.32)$$

$$\mathbf{g}(\alpha_i) = \mathbf{g}_{i+1}, \quad i \in \{0, \dots, N\}. \quad (2.33)$$

Before we introduce a discrete augmented energy functional and show that for such a surface it approximates the continuous Lagrangian to second order in  $h$ , we derive some preliminary identities. We start with applying the Taylor expansion to the discrete isometry constraints (2.18). From the discrete normalization constraint (2.18)<sub>2</sub> of the generatrix  $\mathbf{g}_i$  for  $i \in \{1, \dots, N\}$ , we find that

$$\begin{aligned} 0 &= |\mathbf{g}_{i+1}|^2 - (\mathbf{g}_{i+1} \cdot \mathbf{u}_{i+1})^2 - 1 \\ &= |\mathbf{g}(\alpha_i)|^2 - (\mathbf{g}(\alpha_i) \cdot \mathbf{d}'(\alpha_{i+1/2}))^2 - 1 \\ &= |\mathbf{g}(\alpha_i)|^2 - (\mathbf{g}(\alpha_i) \cdot (\mathbf{d}'(\alpha_i) + h\mathbf{d}''(\alpha_i) + O(h)))^2 - 1 \\ &= |\mathbf{g}(\alpha_i)|^2 - (\mathbf{g}(\alpha_i) \cdot \mathbf{d}'(\alpha_i))^2 - 1 + 2h(\mathbf{g}(\alpha_i) \cdot \mathbf{d}'(\alpha_i))(\mathbf{g}(\alpha_i) \cdot \mathbf{d}''(\alpha_i)) + O(h^2). \end{aligned} \quad (2.34)$$

From the constraint (2.18)<sub>3</sub> that preserves the angle between the discrete midline seg-

## 2.2 Convergence of the discrete functional to the continuous functional 23

ment  $\mathbf{u}_i$  and the discrete generatrix  $\mathbf{g}_i$  for  $i \in \{1, \dots, N\}$ , we obtain

$$\begin{aligned} 0 &= \mathbf{g}_{i+1} \cdot \left( \frac{\mathbf{u}_{i+1} - \mathbf{u}_i}{h} \right) \\ &= \mathbf{g}(\alpha_i) \cdot (\mathbf{d}'(\alpha_{i+1/2}) - \mathbf{d}'(\alpha_{i-1/2})) \\ &= \mathbf{g}(\alpha_i) \cdot \mathbf{d}''(\alpha_i) + O(h^2). \end{aligned} \quad (2.35)$$

Next, from the constraint (2.18)<sub>4</sub> for  $i \in \{0, \dots, N-1\}$ , we find that

$$\begin{aligned} 0 &= \frac{(\mathbf{u}_{i+1} \times \mathbf{g}_{i+1}) \cdot \mathbf{g}_{i+2}}{h} \\ &= \left( \mathbf{u}_i \times \frac{\mathbf{g}_{i+1} + \mathbf{g}_i}{2} \right) \cdot \frac{\mathbf{g}_{i+1} - \mathbf{g}_i}{h} \\ &= (\mathbf{d}'(\alpha_{i+1/2}) \times \mathbf{g}(\alpha_{i+1/2})) \cdot \mathbf{g}'(\alpha_{i+1/2}) + O(h^2). \end{aligned} \quad (2.36)$$

Finally, expansion of the constraint (2.10) that establishes the relation between  $\xi_i$  and the discrete midline  $\mathbf{u}_i$  and generatrix  $\mathbf{g}_i$  for  $i \in \{1, \dots, N\}$  yields

$$\begin{aligned} 0 &= b \mathbf{u}_i \cdot \frac{\mathbf{g}_{i+1} - \mathbf{g}_i}{h} - \tanh \xi_i \\ &= b \mathbf{u}(\alpha_{i+1/2}) \cdot \mathbf{g}'(\alpha_{i+1/2}) - \tanh \xi(\alpha_{i+1/2}) + O(h^2). \end{aligned} \quad (2.37)$$

We can now make some observations regarding the constraints for the continuous optimization problem (1.57). Normalization of the discrete directrix constraint (2.18)<sub>1</sub> leads to  $|\mathbf{d}'| = 1$  exactly at  $\alpha_{i+1/2}$ ,  $i \in \{1, \dots, N\}$ . The decompositions (2.34) and (2.35) yield

$$|\mathbf{g}|^2 - (\mathbf{g} \cdot \mathbf{d}')^2 - 1 = O(h^2) \text{ at } \alpha_i, i \in \{0, N-1\}. \quad (2.38)$$

The decomposition (2.35) gives

$$\mathbf{d}'' \cdot \mathbf{g} = O(h^2) \text{ at } \alpha_i, i \in \{0, N-1\}. \quad (2.39)$$

Similarly, the decomposition (2.36) yields

$$(\mathbf{d}' \times \mathbf{g}) \cdot \mathbf{g}' = O(h^2) \text{ at } \alpha_{i+1/2}, i \in \{0, N-1\}. \quad (2.40)$$

Finally, decomposition of the bilateral injectivity constraint (2.37) gives

$$b \mathbf{u} \cdot \mathbf{g}' - \tanh \xi = O(h^2) \text{ at } \alpha_{i+1/2}, i \in \{0, N-1\}. \quad (2.41)$$

Moreover, the constraints (1.34) are fulfilled everywhere else on  $[0, \ell]$  to the first order in  $h$  if the parametrization of  $\mathcal{S}$  is sufficiently smooth.

Next, consider the following expansion of the midline closure condition (2.17)

$$\begin{aligned}
0 &= \sum_{i=1}^N \mathbf{u}_i \\
&= \sum_{i=1}^N \mathbf{d}'(\alpha_{i+1/2}) \\
&= \sum_{i=1}^N \left\{ \frac{\mathbf{d}(\alpha_{i+1}) - \mathbf{d}(\alpha_i)}{h} + \mathbf{O}(h^2) \right\} \\
&= \frac{1}{h} \left\{ \sum_{i=1}^{N+1} \mathbf{d}(\alpha_i) - \sum_{i=0}^N \mathbf{d}(\alpha_i) \right\} + \mathbf{O}(h) \\
&= \frac{\mathbf{d}(\alpha_{N+1}) - \mathbf{d}(\alpha_1)}{h} + \mathbf{O}(h) \\
&= \frac{\mathbf{d}(\ell) - \mathbf{d}(0)}{h} + \mathbf{O}(h). \tag{2.42}
\end{aligned}$$

Hence, we infer that  $\mathbf{d}(\ell) - \mathbf{d}(0) = \mathbf{O}(h^2)$ .

Next, consider the integrand of the discrete energy functional in the form (2.13):

$$\begin{aligned}
&\left| \frac{\mathbf{u}_{i+1} - \mathbf{u}_i}{h} \right|^2 |g_i|^4 \frac{(\xi_{i+1} + \xi_i)/2}{\tanh((\xi_{i+1} + \xi_i)/2)} \\
&= \left| \frac{\mathbf{u}(\alpha_{i+3/2}) - \mathbf{u}(\alpha_{i+1/2})}{h} \right|^2 |\mathbf{g}(\alpha_{i+1})|^4 \frac{(\xi(\alpha_{i+3/2}) + \xi(\alpha_{i+1/2}))/2}{\tanh(\xi(\alpha_{i+3/2}) + \xi(\alpha_{i+1/2}))/2} \\
&= |\mathbf{u}'(\alpha_{i+1}) + \mathbf{O}(h^2)|^2 |\mathbf{g}(\alpha_{i+1})|^4 \frac{\xi(\alpha_{i+1}) + \mathbf{O}(h^2)}{\tanh(\xi(\alpha_{i+1}) + \mathbf{O}(h^2))} \\
&= |\mathbf{u}'(\alpha_{i+1})|^2 |\mathbf{g}(\alpha_{i+1})|^4 \frac{\xi(\alpha_{i+1})}{\tanh(\xi(\alpha_{i+1}))} + \mathbf{O}(h^2), \quad i \in 1, \dots, N. \tag{2.43}
\end{aligned}$$

Consider intervals  $J_i = [\alpha_{i-1/2}, \alpha_{i+1/2}]$ ,  $i \in 0, \dots, n-1$ . First, from the mean value theorem notice that for each  $i \in \{1, \dots, N\}$  and any sufficiently smooth function  $f$  there exists a choice of  $\xi \in J_i$  such that

$$\int_{\alpha_{i-1/2}}^{\alpha_{i+1/2}} f(\alpha) d\alpha - f(\alpha_i)h = \frac{h^3}{24} f''(\xi). \tag{2.44}$$

We have thus shown that

$$\left| \frac{\mathbf{u}_{i+1} - \mathbf{u}_i}{h} \right|^2 |g_i|^4 \frac{(\xi_{i+1} + \xi_i)/2}{\tanh((\xi_{i+1} + \xi_i)/2)} h = |\mathbf{u}'(\alpha_{i+1})|^2 |\mathbf{g}(\alpha_{i+1})|^4 \frac{\xi(\alpha_{i+1})}{\tanh(\xi(\alpha_{i+1}))} h + \mathbf{O}(h^3), \tag{2.45}$$

where  $i \in \{1, \dots, N\}$ . Hence, taking into account the periodicity of  $\mathbf{u}$  and  $\mathbf{g}$  and

performing integration,

$$\begin{aligned}
Q_h &= \sum_{i=1}^N q_i r_i a_i / h \\
&= \sum_{i=0}^{N-1} (|\mathbf{u}'(\alpha_{i+1})|^2 |\mathbf{g}(\alpha_{i+1})|^4 \frac{\xi(\alpha_{i+1})}{\tanh(\xi(\alpha_{i+1}))} h + \mathbf{O}(h^3)) \\
&= \sum_{i=0}^{N-1} \left( \int_{\alpha_{i-1/2}}^{\alpha_{i+1/2}} |\mathbf{u}'|^2 |\mathbf{g}|^4 \frac{\xi}{\tanh \xi} d\alpha + \mathbf{O}(h^3) \right) \\
&= \int_0^\ell |\mathbf{u}'|^2 |\mathbf{g}|^4 \frac{\xi}{\tanh \xi} d\alpha + \mathbf{O}(h^2) \tag{2.46}
\end{aligned}$$

we arrive at an approximation of the continuous energy by the discrete one that is accurate to second-order in  $h$ .

Next, we introduce Lagrange multipliers  $\lambda_{1i}, \lambda_{2i}, \lambda_{3i}, \lambda_{4i}, \lambda_{5i}$ , for  $i \in \{1, \dots, N\}$ . Finally, we can introduce the discrete Lagrangian  $\mathcal{L}_D$  in the form

$$\begin{aligned}
\mathcal{L}_D &= \sum_{i=1}^N \left[ q_i \rho_i^4 a_i / h - \lambda_{1i} (|\mathbf{u}_i| - 1) h - \lambda_{2i} (|\mathbf{g}_i|^2 - (\mathbf{g}_i \cdot \mathbf{u}_i)^2 - 1) h - \right. \\
&\quad \left. - \lambda_{3i} (\mathbf{u}_i - \mathbf{u}_{i-1}) \cdot \mathbf{g}_i - \lambda_{4i} (\mathbf{u}_i \times \mathbf{g}_i) \cdot \mathbf{g}_{i+1} - \lambda_{5i} (b \mathbf{u}_i \cdot (\mathbf{g}_{i+1} - \mathbf{g}_i) - h \tanh \xi_i) \right] - \\
&\quad - \lambda_{5N+1} \sum_{i=1}^N u_{ix} h - \lambda_{5N+2} \sum_{i=1}^N u_{iy} h - \lambda_{5N+3} \sum_{i=1}^N u_{iz} h, \tag{2.47}
\end{aligned}$$

where  $\mathbf{u}_i = (u_{ix}, u_{iy}, u_{iz})$  in some Cartesian coordinates.

We construct continuous scalar Lagrange multipliers fields  $\lambda_1, \lambda_2, \lambda_3, \lambda_4, \lambda_5$  such that they satisfy

$$\begin{aligned}
\lambda_1(\alpha_{i+1/2}) &= \lambda_{1i}, & \lambda_2(\alpha_i) &= \lambda_{2i}, & \lambda_3(\alpha_i) &= \lambda_{3i}, \\
\lambda_4(\alpha_{i+1/2}) &= \lambda_{4i}, & \lambda_5(\alpha_{i+1/2}) &= \lambda_{5i}. \tag{2.48}
\end{aligned}$$

As the choice of the points where discrete Lagrange multipliers coincide with their continuous counterpart is in agreement with the points where the discrete constraints approximate the continuous counterparts with the second order, we can apply the mean value theorem (2.44) to each term of the Lagrangian and conclude that it approximates the continuous one to the second order in  $h$ .

## 2.3 Saddle-free Newton method

Having obtained the discrete optimization problem and showed that it quadratically converges to the continuous problem as the step-size  $h$  is reduced, we need a strategy for solving that problem. One approach to doing so relies on the sequential quadratic programming method, which is a standard Newton method but for nonlinear constrained

optimization problems. A detailed derivation and theoretical study of this method can be found in the book of Nocedal and Wright [18]. However, this method has an issue that is present when dealing with constrained or unconstrained optimization problems. The classical Newton method is a very effective tool for convex optimization but requires modification for nonconvex problems. In particular, Newton's method often converges to saddle points that are in abundance in high-dimensional nonconvex problems. One way of obtaining a modification that is saddle-free has been proposed by Dauphin *et al.* [20] for unconstrained optimization. In this section, we will first summarize how the saddle-free method works for unconstrained optimization and then generalize it to the constrained optimization case.

### 2.3.1 Unconstrained optimization

Let us first describe the basic features of the standard saddle-free method and then generalize that method for the case of constrained optimization.

Consider the following unconstrained optimization problem

$$\min f(\mathbf{x}), \quad (2.49)$$

where  $f$  is a scalar field and  $\mathbf{x}$  a point  $n$ -dimensional vector space. The standard Newton approach (minimizing second order approximation of  $f$ ) to tackle the problem leads to the iterative process

$$\mathbf{x}^{k+1} = \mathbf{x}^k - \mathbf{H}^{-1}(\nabla f(\mathbf{x}^k)) \quad (2.50)$$

where  $\mathbf{H} = \nabla \nabla f|_{\mathbf{x}=\mathbf{x}^k}$  is a symmetric tensor-valued field and thus admits the eigenvalue decomposition

$$\mathbf{H} = \mathbf{Q}^T \mathbf{\Sigma} \mathbf{Q}, \quad (2.51)$$

where  $\mathbf{Q}$  is orthogonal the tensor form from the eigenvectors of  $\mathbf{H}$  and  $\mathbf{\Sigma}$  is a diagonal tensor composed from the eigenvalues of  $\mathbf{H}$ . In the saddle-free modification,  $\mathbf{H}$  is replaced by  $\hat{\mathbf{H}} = \mathbf{Q}^T \hat{\mathbf{\Sigma}} \mathbf{Q}$ , where  $\hat{\mathbf{\Sigma}}$  is obtained from  $\mathbf{\Sigma}$  by replacing each eigenvalue of  $\mathbf{\Sigma}$  with its absolute value. This approach can help to avoid saddle points in non-convex unconstrained optimization. To explain this, it is helpful to first mention why the standard Newton method converges to saddle points. As explained in Dauphin *et al.* [20] using Morse's lemma (chapter 7.3, Theorem 7.16 in Callahan [23]), near a critical point  $\mathbf{x}^*$  the scalar function  $f(\mathbf{x})$  can be reparametrized as

$$f(\mathbf{x}^* + \mathbf{p}) = f(\mathbf{x}^*) + \frac{1}{2} \mathbf{v} \cdot \mathbf{\Sigma} \mathbf{v},$$

where  $\mathbf{\Sigma}$  is the diagonal matrix with diagonal elements  $\sigma_i$  obtained from the Hessian's eigendecomposition  $\mathbf{H} = \mathbf{Q}^T \mathbf{\Sigma} \mathbf{Q}$ ,  $\sigma_i$  is  $i$ -th eigenvalue along the Hessian's eigenvector  $\mathbf{e}_i$  and  $\mathbf{v} = \mathbf{Q} \mathbf{p} = \sum_{i=1}^n v_i \mathbf{e}_i$ . Thus, in this coordinates the Newton method has a step  $-v_i$  along  $\mathbf{e}_i$ . It is now clear that classical Newton method will move towards a saddle point in the eigendirections of the Hessian at which the corresponding eigenvalue is negative. This happens due to the fact that while scaling out the curvature of  $f$ , not only the absolute value is scaled out but also the sign of the curvature. On the

other hand, the gradient descent preserves  $\sigma_i$  and has a step  $-\sigma_i \mathbf{v}_i$  along  $\mathbf{e}_i$ . Thus, the gradient descent method repels from saddle points, but might take long time if the landscapes is flat (absolute value of  $\sigma_i$  is small). The modification of the Hessian described above allows to only scale out the absolute value and the step is  $-\sigma_i/|\sigma_i| \mathbf{v}_i$  along  $\mathbf{e}_i$ , and thus, the modified method will repel from saddle points. Scaling out the absolute value is advantageous as we do not want the iterations to get stuck at flat landscapes near critical points. Dauphin *et al.* [20] also show that the approach performs well in practical applications.

### 2.3.2 Constrained optimization

Consider now the optimization problem with equality constraints

$$\min f(\mathbf{x}), \quad \text{subject to } \mathbf{c}(\mathbf{x}) = \mathbf{0}_m, \quad (2.52)$$

where  $f$  is still a scalar field and  $\mathbf{c}$  is a vector field from  $n$  dimensional vector space into  $m$  dimensional vector space. One common way to deal with such an optimization problem is to introduce the  $m$ -dimensional vector field  $\boldsymbol{\lambda}$  of Lagrange multipliers and consider the augmented functional

$$\mathcal{L}(\mathbf{x}, \boldsymbol{\lambda}) = f(\mathbf{x}) - \boldsymbol{\lambda} \cdot \mathbf{c}(\mathbf{x}). \quad (2.53)$$

Let  $\mathbf{y}^k$  be a vector in  $n + m$  dimensional vector space that combines  $\mathbf{x}^k$  and  $\boldsymbol{\lambda}^k$ . Now the first and second order conditions of a minimum can be written in a concise way. The first order condition simply reads

$$\nabla_{\mathbf{y}} \mathcal{L}(\mathbf{y}^*) = \mathbf{0}. \quad (2.54)$$

Next, we introduce

$$\mathbf{W} = \nabla_x \nabla_x f(\mathbf{x}^k) - (\nabla_x \nabla_x \mathbf{c}(\mathbf{x}^k)) \boldsymbol{\lambda} \quad (2.55)$$

Then the standard Newton approach for the constrained optimization will lead to the iterative process called Sequential Quadratic Programming (SQP, [18])

$$\mathbf{y}^{k+1} = \mathbf{y}^k - \mathbf{J}^{-1} \nabla_{\mathbf{y}} \mathcal{L}(\mathbf{y}^k), \quad (2.56)$$

where  $\mathbf{J} = \nabla_{\mathbf{y}} \nabla_{\mathbf{y}} \mathcal{L}(\mathbf{y}^k)$ . In a matrix form,  $\mathbf{J}$  consists of the following blocks

$$\mathbf{J} = \begin{bmatrix} \mathbf{W} & \nabla_{\boldsymbol{\lambda}} \mathbf{c}(\mathbf{x}^k) \\ (\nabla_{\boldsymbol{\lambda}} \mathbf{c}(\mathbf{x}^k))^{\top} & \mathbf{0}_{m,m} \end{bmatrix} \quad (2.57)$$

Now, let  $\mathbf{K}$  be combined of the  $m$  vectors in  $n$ -dimensional vector space that form the null space of  $\nabla_{\boldsymbol{\lambda}} \mathbf{c}(\mathbf{x}^k)$  (and thus must have rank  $m$ , meaning that there are  $m$  linearly independent  $n$ -dimensional vectors that do not annihilate  $\mathbf{c}(\mathbf{x})$ ). For the second order condition, we need to introduce

$$\mathbf{W}_c = \mathbf{K}^{\top} \mathbf{W} \mathbf{K}. \quad (2.58)$$

If the constraints are linearly independent at  $\mathbf{x}^*$  corresponding to  $\mathbf{y}^*$ , then the solution  $\mathbf{y}^*$  is a (strict) minimum if  $\mathbf{W}_c$  is (strictly) positive-definite.

As it is discussed in detail in Nocedal and Wright book [18], the matrix  $\mathbf{K}$  is used to restrict the function  $f(\mathbf{x})$  to change only in the allowed directions (allowed direction must not change the value of  $\mathbf{c}(\mathbf{x}^*)$  and thus must be orthogonal to  $\mathbf{c}(\mathbf{x}^*)$  that is  $\mathbf{K}$  by its definition). Thus, we can perform analogous modularization of the constrained Hessian  $\mathbf{W}_c$  at each step as it is done in unconstrained case. The only issue is that to next perform the SQP step we need to return to the original space, but  $\mathbf{K}$  is not invertible. However, it is easy to fix by appending  $\mathbf{K}$  with the matrix containing the value of the gradient of the constraints. Namely, we introduce  $\mathbf{T} = (\mathbf{K}|\nabla\mathbf{c})$  to get

$$\mathbf{T}^\top \nabla^2 \mathcal{L} \mathbf{T} = \begin{bmatrix} \mathbf{H}_c & \cdots \\ \cdots & \cdots \end{bmatrix}. \quad (2.59)$$

As  $\mathbf{T}$  is invertible, we can now return to the original space by applying it to the right hand side of (2.59). We now summarize the saddle-free Newton approach in the next paragraph.

To obtain the saddle-free Newton method for constrained optimization, in analogy with the unconstrained method, we modify  $\mathbf{W}_c$  into  $\hat{\mathbf{W}}_c$  by replacing the negative eigenvalue with its absolute values. Next, we write  $\mathbf{W}$  in coordinates aligned with the null space of  $\nabla_\lambda \mathbf{c}(\mathbf{x}^k)$  and replace any block of coordinates corresponding to  $\mathbf{W}_c$  with the coordinates for  $\hat{\mathbf{W}}_c$  and denote the result by  $\hat{\mathbf{W}}$ . Using  $\hat{\mathbf{J}}$  to denote  $\mathbf{J}$  with  $\hat{\mathbf{W}}$  instead of  $\mathbf{W}$ , we now perform the iteration step as in the standard Newton method, but using  $\hat{\mathbf{J}}$  instead of  $\mathbf{J}$ . We call this algorithm the saddle-free Newton method for constrained optimization. As the algorithm involves essentially the same modification to the projected Hessian  $\mathbf{W}_c$  in the constrained space as the original unconstrained algorithm does to the unconstrained Hessian  $\mathbf{H}$ , we believe that it should help to avoid saddle-points in constrained optimization problems. The method has proven effective in practice; the results in the next chapter were obtained using this method.

# Chapter 3

## Numerical results

In this chapter, we consider bands with three different topologies: bands with untwisted short ends, namely bands with cylindrical topology; bands with short edges twisted once, namely standard  $\pi$ -twisted Möbius bands; and bands with short edges twisted three times, namely  $3\pi$ -twisted Möbius bands. In Section 3.1 we provide general strategies of obtaining the discrete solution. As the numerical approach we developed in the previous section is iterative, having reasonable initial guesses is crucial for computing a desired solution. Thus, for each of the bands we first present the process of obtaining the initial guess. For each band we next plot numerical approximations of the quantities

$$\kappa_s = \mathbf{d}'' \cdot (\mathbf{g}' \times \mathbf{d}'), \quad \tau = \kappa_s \eta, \quad \eta = \mathbf{d}' \cdot \mathbf{g} \quad \text{and} \quad \eta' = \mathbf{d}' \cdot \mathbf{g}', \quad (3.1)$$

as well as the Lagrange multipliers. Additionally, we discuss the issues concerning the relationship between the stability of the discrete solutions and the continuous counterpart. Finally, we provide some *a posteriori* convergency results theoretically established in the previous chapter.

### 3.1 Numerical strategies

There are three main strategies that we use to obtain numerical results. First, we need to obtain an initial guess for a solution on a coarse grid. Thus, for each of the three topologies considered, we first present an approach to obtain a reasonable initial guess. To obtain an initial guess, we prescribe positions of some generators  $\mathbf{g}_i$  without assigning any physical meaning to this boundary conditions. Once we obtain an initial guess, we perform numerical iterations using the saddle-free Newton method developed in Subsection 2.3.2 to obtain a local minimum for a coarse grid.

Second, having a coarse minimum, we move to the second step — refining the discretization. Suppose we have a local minimum for the number of flat segments  $N$  equal  $N^*$ . Let us demonstrate the process of refining the discretization. To do so, we split each of the flat segments of the coarsely discretized band obtained into two, so that the two normalized midline vectors  $\mathbf{u}_{i-1/2}$  and  $\mathbf{u}_{i+1/2}$  coincide with the original midline  $\mathbf{u}_i$ , and the new ruling  $\mathbf{g}_{i+1/2}$  in the center is the average of  $\mathbf{g}_i$  and  $\mathbf{g}_{i+1}$ . We then use the new set of discrete midline vectors  $\mathbf{u}_i$ ,  $i \in \{1, \dots, 2N^*\}$ , and generators

$\mathbf{g}_i$ ,  $i \in \{1, \dots, 2N^* + 1\}$ , as an initial guess to run the saddle-free algorithm for the optimization problem (2.19) for the band resolved into  $2N^*$  flat segments.

Finally, having obtained a solution for given half-width  $b^*$ , we can obtain a solution for a different half-width  $b^{**}$ . To do so, we use an incremental process where a solution for the previous width is used as an initial guess for another width. Specifically, we consider,

$$b_0 = b^*, \quad (3.2)$$

$$b_{j+1} = b_j + \frac{b^{**} - b^*}{M}, \quad j \in 0, \dots, M - 1. \quad (3.3)$$

for some positive integer  $M$ . Thus,  $b_M = b^{**}$  and we obtain a solution for the required width. This process would not be possible for  $b^{**} > b^*$  without introducing the bilateral constraint as the energy functional (1.48) in this case would not be finite for  $b = b^{**}$ .

Also, as there is only one dimensionless parameter in the problem — namely the width to length aspect ratio  $2b/\ell$ , we fix the length for all bands considered to be  $2\pi$ . Next, we vary the width to study how the aspect ratio affects the solution.

## 3.2 Cylindrical band

### 3.2.1 Initial guess

For the untwisted topology, we have one obvious minimum: the right-circular cylindrical shape. This shape is easy to construct and use as an initial guess. However, the outcome from applying the numerical approach developed in Chapter 2 will be also a cylindrical ring as it is a minimum. We thus start from the cylinder but obtain a different initial guess that is closer to the partially everted cylinder by subjecting it to certain isometric modifications that we next describe. See also Figures 3.1, 3.2.

Consider an orthonormal basis  $\{\mathbf{v}_1, \mathbf{v}_2, \mathbf{v}_3\}$  for three dimensional Euclidean vector space. First, we construct a discrete counterpart of a right-circular cylinder with its axis of symmetry aligned along  $\mathbf{v}_3$ . Thus, all of the generators  $\mathbf{g}_i$ ,  $i \in \{1, \dots, N + 1\}$ , are aligned along  $\mathbf{v}_3$  and of unit magnitude. The midline vectors  $\mathbf{u}_i$ ,  $i \in \{1, \dots, N\}$ , should form a closed right polygon in the plane spanned by  $\mathbf{v}_1$  and  $\mathbf{v}_2$ . Thus, the midline vectors and generators can be written in the form

$$\mathbf{u}_i = \cos \frac{2\pi(i - 0.5)}{N} \mathbf{v}_1 + \sin \frac{2\pi(i - 0.5)}{N} \mathbf{v}_2, \quad i \in \{1, \dots, N\}, \quad (3.4)$$

$$\mathbf{g}_i = \mathbf{v}_3, \quad i \in \{1, \dots, N + 1\}. \quad (3.5)$$

We next iteratively isometrically deform the surface by prescribing of two generators and solving the optimization problem with this additional control. We take two diametrically opposed rulings that are initially parallel and incrementally rotate each of them by a total angle of  $\pi/2$  to become antiparallel. In particular, assuming that the number of flat segments  $N$  is an even number, we prescribe generators  $\mathbf{g}_1$  and  $\mathbf{g}_{N/2+1}$

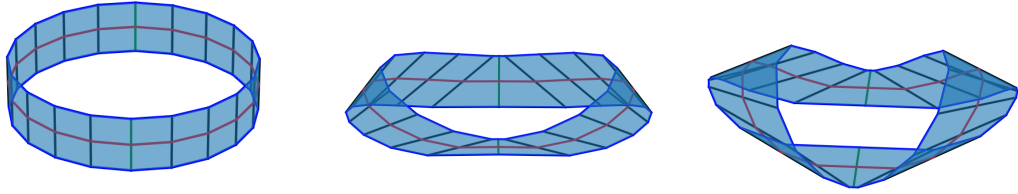


**Figure 3.1:** Auxiliary incremental process to obtain the initial guess for a partially everted cylinder for  $K = 25$  (see (3.8)) and number of flat segments  $N = 20$ . The generators  $\mathbf{g}_1$  and  $\mathbf{g}_{11}$  are marked green. The figure on the left corresponds to  $k = 0$  (discrete cylindrical ring); in the center,  $k = 13$ ; on the and in right,  $k = 25$ .

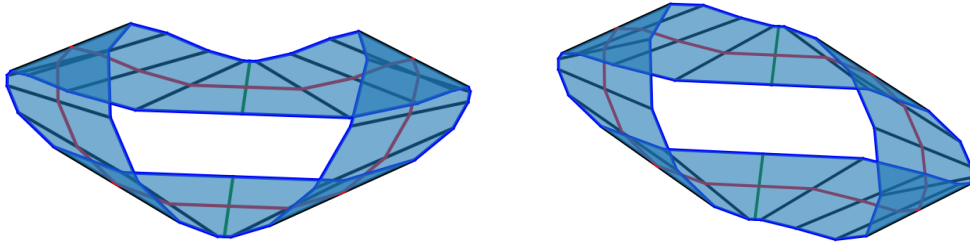


**Figure 3.2:** Auxiliary process of rotating half of the band to obtain initial guess for the partially everted cylinder for  $K = 25$  and  $N = 20$ . The generators  $\mathbf{g}_1$  and  $\mathbf{g}_{21}$  are marked green.

by the rule

$$\mathbf{g}_1 = \sin \varphi_k \mathbf{v}_2 + \cos \varphi_k \mathbf{v}_3 \quad (3.6)$$

$$\mathbf{g}_{N/2+1} = -\sin \varphi_k \mathbf{v}_2 + \cos \varphi_k \mathbf{v}_3, \quad (3.7)$$

where

$$\varphi_k = \frac{\pi k}{2K}, \quad k \in \{0, \dots, K\}, \quad (3.8)$$

and  $K$  is some positive integer. We consequently solve the problem (2.19) for  $\varphi_k$ , using the results for  $\varphi_{k-1}$  as an initial guess. We do not invest physical meaning in the solutions of this auxiliary problem, but merely use them as as reasonable initial guesses. From (3.7), we notice that the discrete counterpart of the right-circular cylinder corresponds to  $k = 0$ .

When the solution is obtained for  $k = K$ , we cut the band along the rulings  $\mathbf{g}_1$  and  $\mathbf{g}_{N/2+1}$ . Next, we rotate half of the band around  $\mathbf{v}_1$  by the angle  $\pi$ . Finally, we smoothly connect the opposite short edges of the band together to obtain the initial guess for the partially everted cylinder.

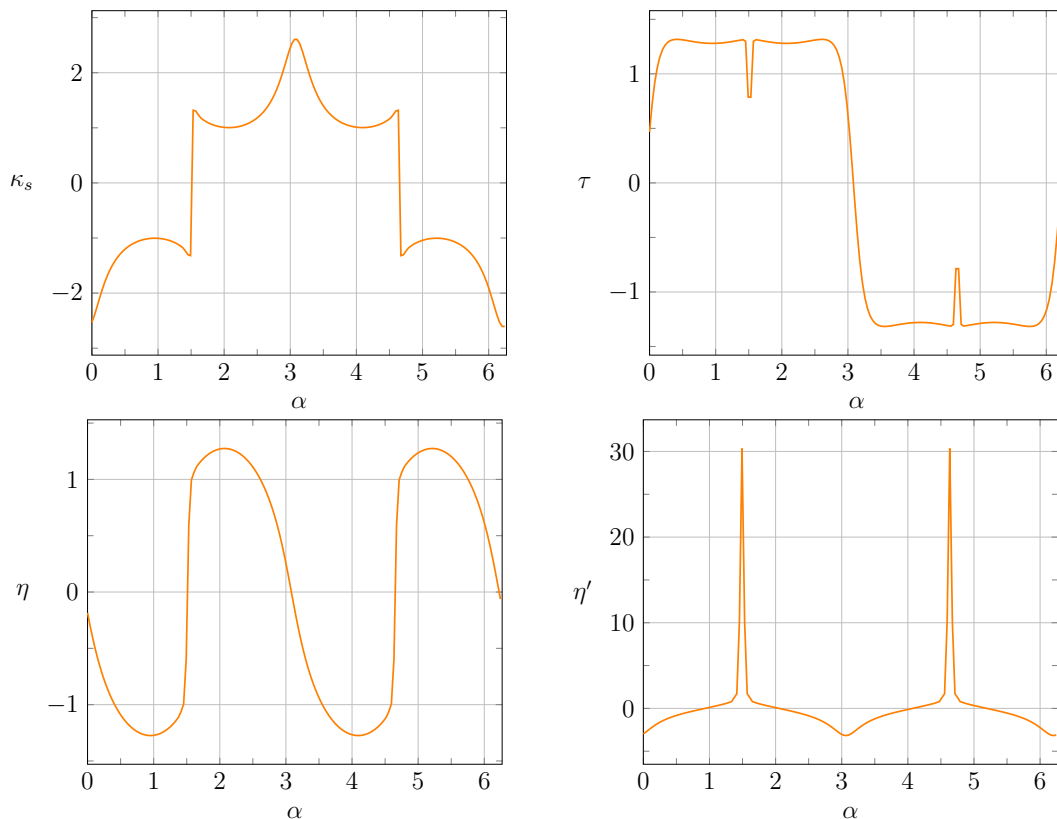


**Figure 3.3:** Geometric properties of the discrete partially everted cylinder for  $b = 0.03$ .

### 3.2.2 Results and analysis

As we already mentioned, the cylindrical configuration is an obvious global energy minimum for a band with cylindrical topology. Thus, if the initial guess is “far” from the local minimum, it is likely to converge to the global one. This explains why we were not able to obtain the finer discretized band that is shown in Figure 3.5. We were also not able to obtain wider partially everted cylinder for given  $N = 160$ . Each time we applied the incremental strategies described in Section 3.1, the iterations converged to a right-circular cylindrical configuration. Hence, here we present only one partially everted discrete cylindrical configuration.

In Figure 3.3, we can see that there are two points  $\alpha \approx 1.5$  and  $\alpha \approx 4.7$  where the signed curvature  $\kappa_s$  vanishes. At the same time, the torsion  $\tau$  diminishes. Although the torsion does not drop to  $\tau = 0$ , this might be due to the coarse discretization. The two points seem to correspond to the flat straight line segments where the mean curvature vanishes that, as proved by Hornung [19], are the only possible flat portions of the minimizer. Also, in the Figure 3.4 we see that at these points the Lagrange multipliers  $\lambda_2$  and  $\lambda_4$  and  $\lambda_5$  reach their maximum absolute values.

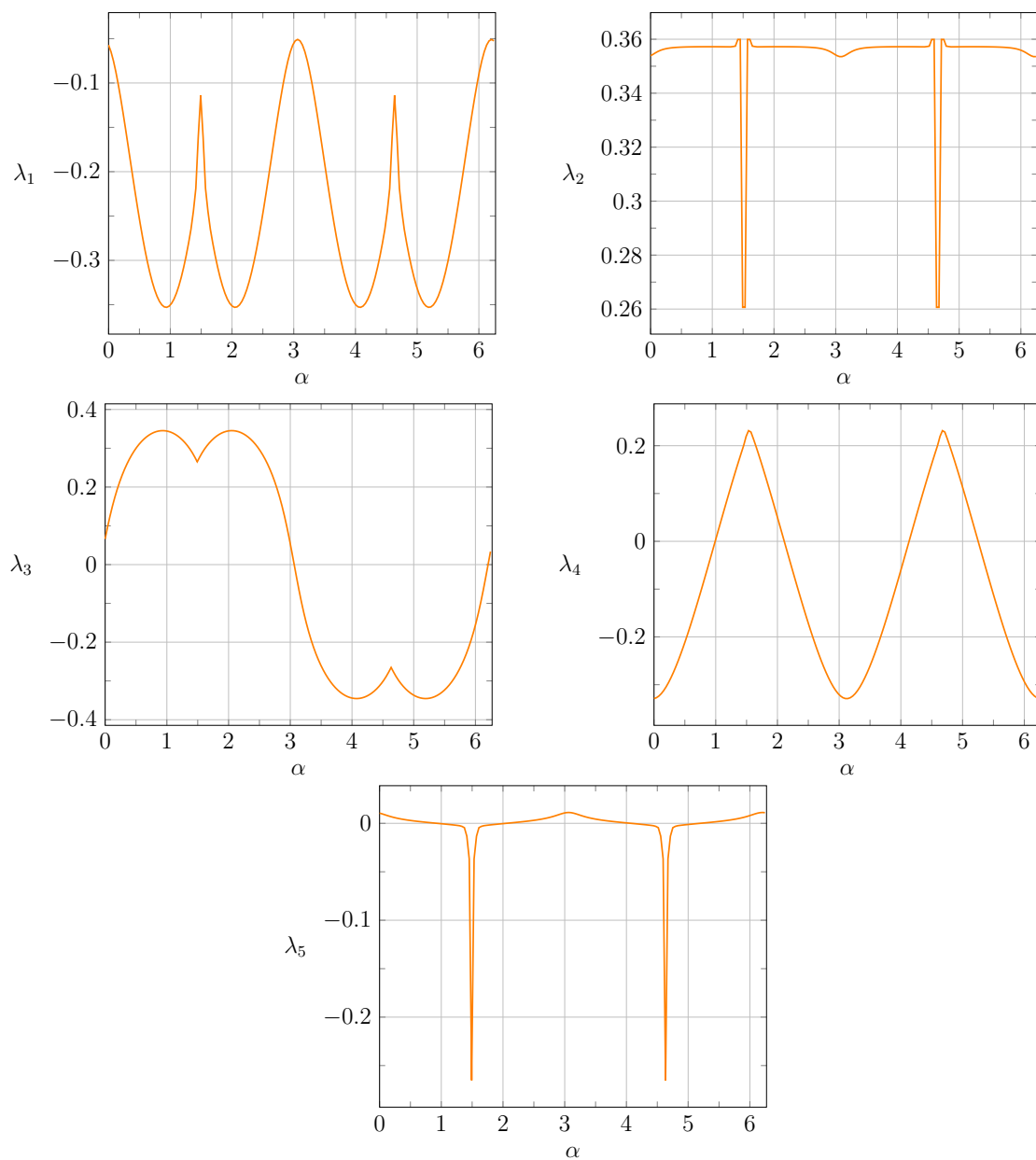


**Figure 3.4:** Lagrange multipliers of the discrete partially everted cylinder for  $b = 0.03$ .

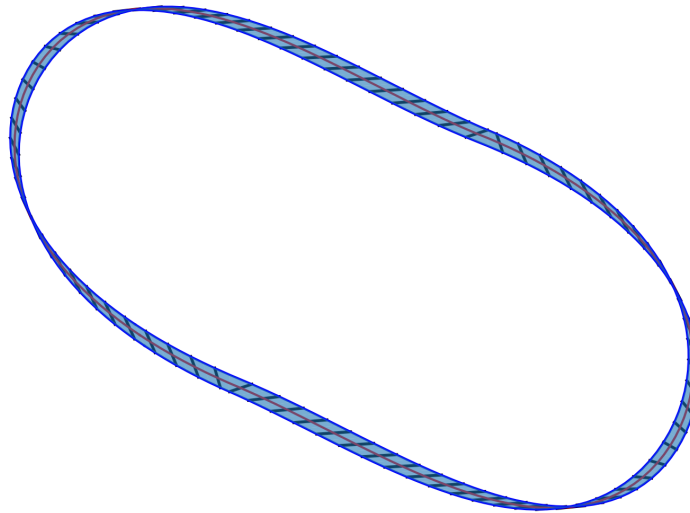


**Figure 3.5:** The shape of the partially everted cylinder for  $N = 160$  and  $b = 0.03$ . Only half of the generators are shown in the picture.

### 3.3 $\pi$ -twisted Möbius band

#### 3.3.1 Initial guess

To construct the initial guess for the  $\pi$ -twisted band, we could use the construction provided by Sadowsky [10]. However, there is another approach that yields an initial guess that is visually closer to an equilibrated  $\pi$ -twisted band. The strategy for constructing this initial guess is based on solving a set of auxiliary problems. For this we need to allow the generators  $\mathbf{g}_1$  and  $\mathbf{g}_{N+1}$  to differ. We start from the initial discrete cylinder (3.5) and rotate  $\mathbf{g}_{N+1}$  while keeping  $\mathbf{g}_1$  fixed. Again, we do not ascribe any physical interpretation to the interim configurations of the band. The incremental process of rotating  $\mathbf{g}_{N/2+1}$  can be written in the form

$$\mathbf{g}_1 = \mathbf{v}_3 \tag{3.9}$$

$$\mathbf{g}_{N/2+1} = \sin \varphi_k \mathbf{v}_2 + \cos \varphi_k \mathbf{v}_3, \tag{3.10}$$

where  $\varphi$  is as in (3.8), but the parameter  $k$  now ranges from 0 (discrete cylinder) to  $2K$ . The final configuration correspond to the case where  $\mathbf{g}_1$  and  $\mathbf{g}_{N+1}$  are antiparallel and visually resembles a Möbius band made of paper (see Figure 3.6).

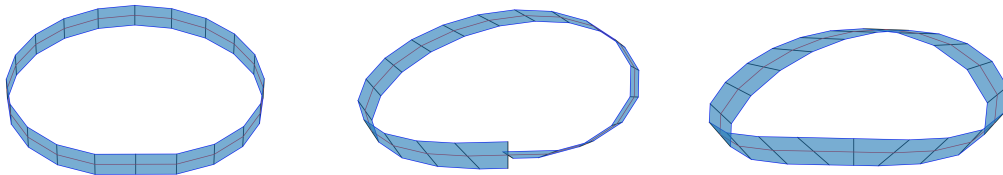


**Figure 3.6:** The process of constructing an initial guess for a  $\pi$ -twisted Möbius band from a cylindrical ring.

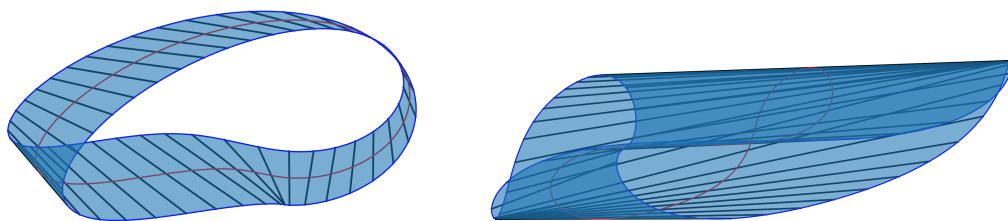


**Figure 3.7:** Examples of  $\pi$ -twisted Möbius bands of width  $b = 0.3$  (left) and almost maximum width  $b = 1.5$  (right). Both of the bands are converged minima of the optimization problem (2.19).

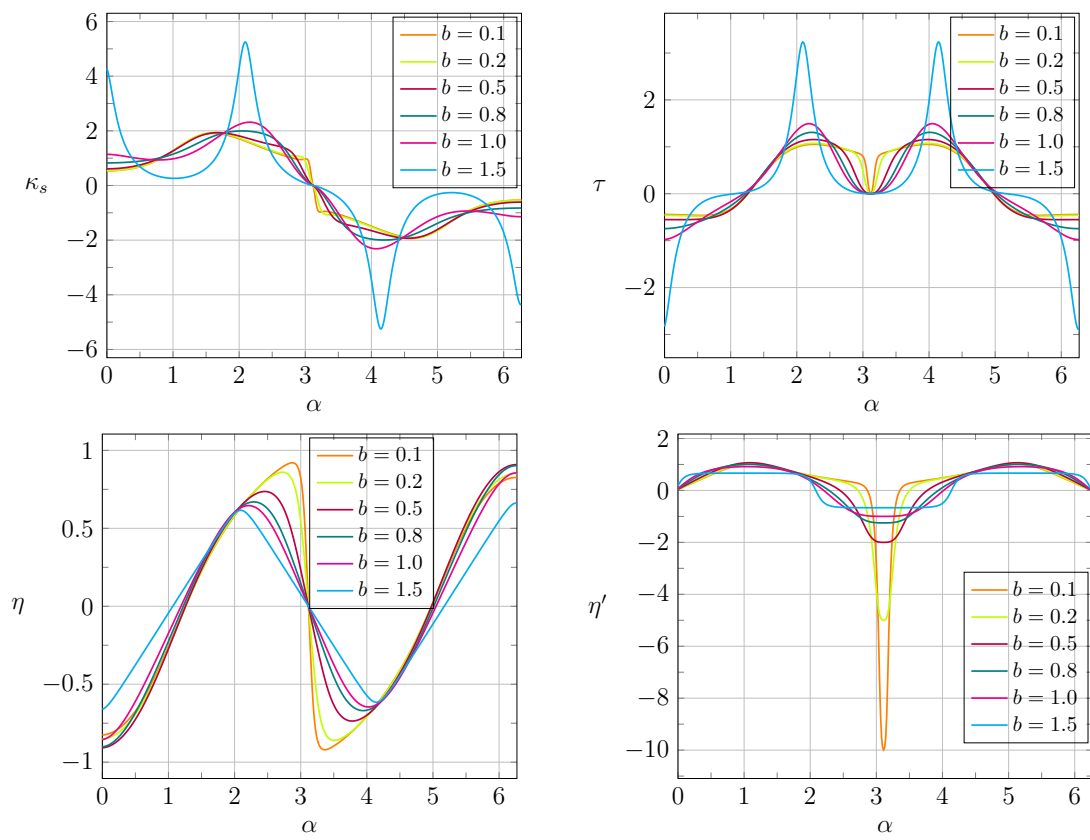


**Figure 3.8:** Geometric properties of the  $\pi$ -twisted Möbius bands.

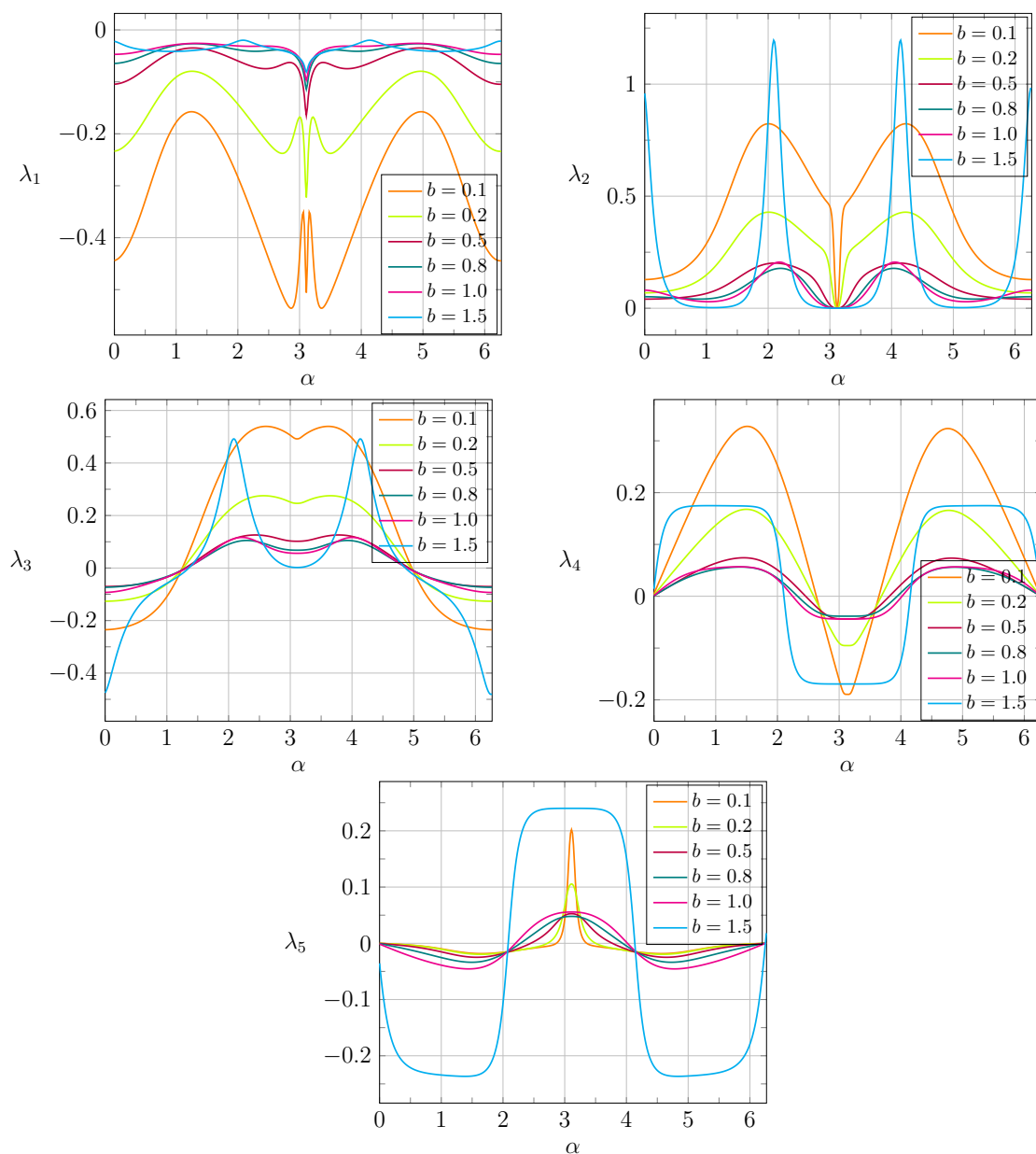


**Figure 3.9:** Lagrange multipliers of the  $\pi$ -twisted Möbius bands.

### 3.3.2 Results and analysis

Unlike the partially everted cylinder, the conventional shapes of the Möbius band shown in Figure 3.7 are likely global minima and thus we did not experience the difficulties with the incremental processes we faced with the partially everted cylindrical configuration. The only limitation for the  $\pi$ -twisted Möbius bands is the aspect ratio at which the band starts to experience self-penetration and thus the deformation is not injective and beyond the scope of this study. For the fixed length  $2\pi$ , the critical half-width for which the minimizer has no self-penetration was found to be  $b = 1.5$ . This result is in agreement with the results by Starostin and van der Heijden [13]. Additionally, the results for the curvature and torsion shown in Figure 3.8 are qualitatively the same as those in Starostin and van der Heijden [13]. The results for  $\eta$  and  $\eta'$  are qualitatively the same as those of Moore and Healey [15]. It is impossible to conduct a quantitative comparison given the information provided in those papers. In Figures 3.8 and 3.9 we also observe  $\pi$ -periodicity of the torsion  $\tau$  and antiperiodicity of the signed curvature  $\kappa_s$ . This supports the flip symmetry assumption made in both Starostin and van der Heijden [13] and Moore and Healey [15] studies. However, the periodicity (antiperiodicity) we observe is not an assumption, but an outcome of numerical computation.

We also observe an inflection point at the Möbius band at  $\alpha \approx \pi$ . Both the curvature and torsion at this point vanish. We also find that each Lagrange multiplier  $\lambda_i$ ,  $i \in \{1, \dots, 5\}$  exhibits a local extremum at this point. In particular,  $\lambda_5$  reaches its global maximum at the critical point. This is in agreement with the results of Hornung [19] that the injectivity constraint is nearly active close to an inflection point.

## 3.4 $3\pi$ -twisted Möbius band

### 3.4.1 Initial guess

For this band we will use another approach to construct the initial guess. Looking at the previous section, it is reasonable to assume that the initial guess for a  $3\pi$ -twisted band might be obtained by twisting the short edges by  $3\pi$  relative to each other, as it was done in the case of a  $\pi$ -twisted band. However, this approach has drawbacks. As we already mentioned, the injectivity constraint is local and cannot prevent global self-contact. Thus, while trying to twist the short edges relative to each other by  $3\pi$ , the band passes through itself and the resulting band is not  $3\pi$  twisted, but  $-\pi$  twisted. We can, however, capitalize on recent work by Schönke *et al.* [1] that amounts to a generalization of Sadowsky's [10] construction for  $\pi$ -twisted bands. In Schönke *et al.* [1], a  $3\pi$ -twisted developable Möbius band is constructed from flat and cylindrical segments as shown in Figure 3.10. We adjust the number of generators within the flat portions of the construction so that all of the discrete isometry constraints, in particular  $|\mathbf{d}_i| = 1$ , are satisfied.

### 3.4.2 Results and analysis

As with the  $\pi$ -twisted Möbius band, for a fixed length  $3\pi$  Möbius band we have a restriction for the half-width  $b$  of the band at which it comes to a self-contact that is

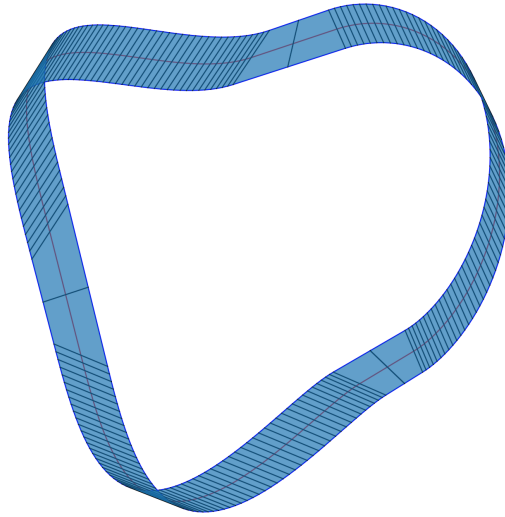


**Figure 3.10:** Initial guess from Schönke *et al.* [1]

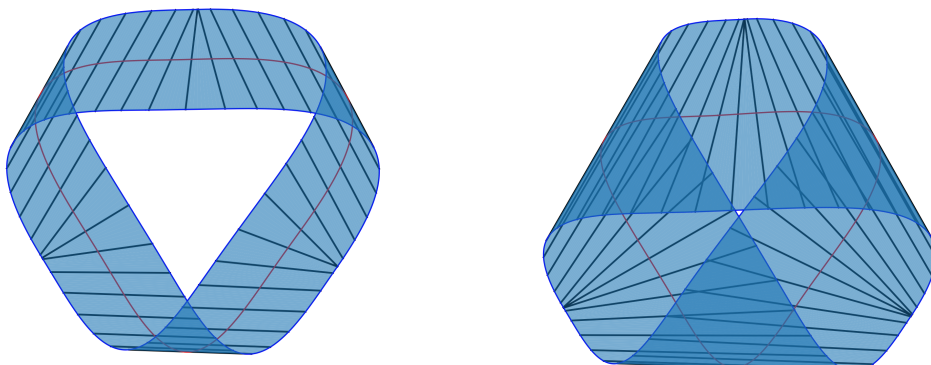


**Figure 3.11:** Examples of  $3\pi$ -twisted Möbius band of width  $b = 0.3$  (left) and almost maximum width  $b = 0.65$  (right).

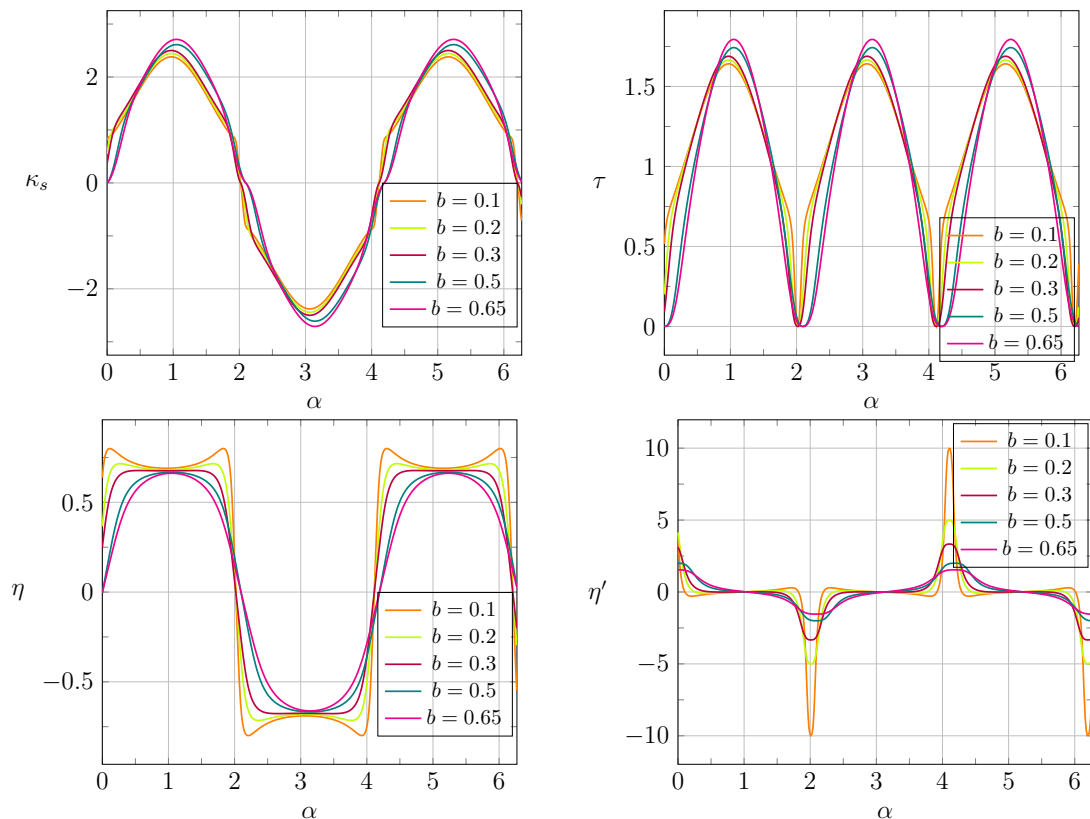


**Figure 3.12:** Geometric properties of the  $3\pi$ -twisted Möbius bands.

effectively a restriction for the half-width to length aspect ratio. For the  $3\pi$ -twisted Möbius band, the contact appears in the center (see Figure 3.11) of the band. The widest band for which the deformation is injective has the half-width  $b \approx 0.65$ . From  $2\pi/3$ -antiperiodicity of the signed curvature  $\kappa_s$  and  $2\pi/3$ -periodicity torsion Figures 3.12 and 3.13, we see that the band consists of three identical parts. Thus, our numerical results also support the existence of a symmetric solution assumed by Starostin and van der Heijden [14]. However, experiments with paper strips suggest that there are other non-symmetric minima, but we were not able to approach them as those minima exhibit self-contact. Also, the  $3\pi$  twisted band has three inflection points at which the Lagrange multipliers  $\lambda_i$ ,  $i \in \{1, \dots, 5\}$  reach a local extremum.

### 3.5 Implications on the stability of the continuous solution

As we checked the eigenvalues of the projected Hessian (2.58) and they are all positive, we claim that all of the discrete bands obtained in previous sections are local minimizers of the discrete optimization problem (2.19). However, the original goal is to obtain local minima of the continuous model. In this section we discuss the challenges arising while attempting to make a connection between the stability of the discrete and continuous bands. For this purpose, we consider a cylindrical band for the number of flat segments

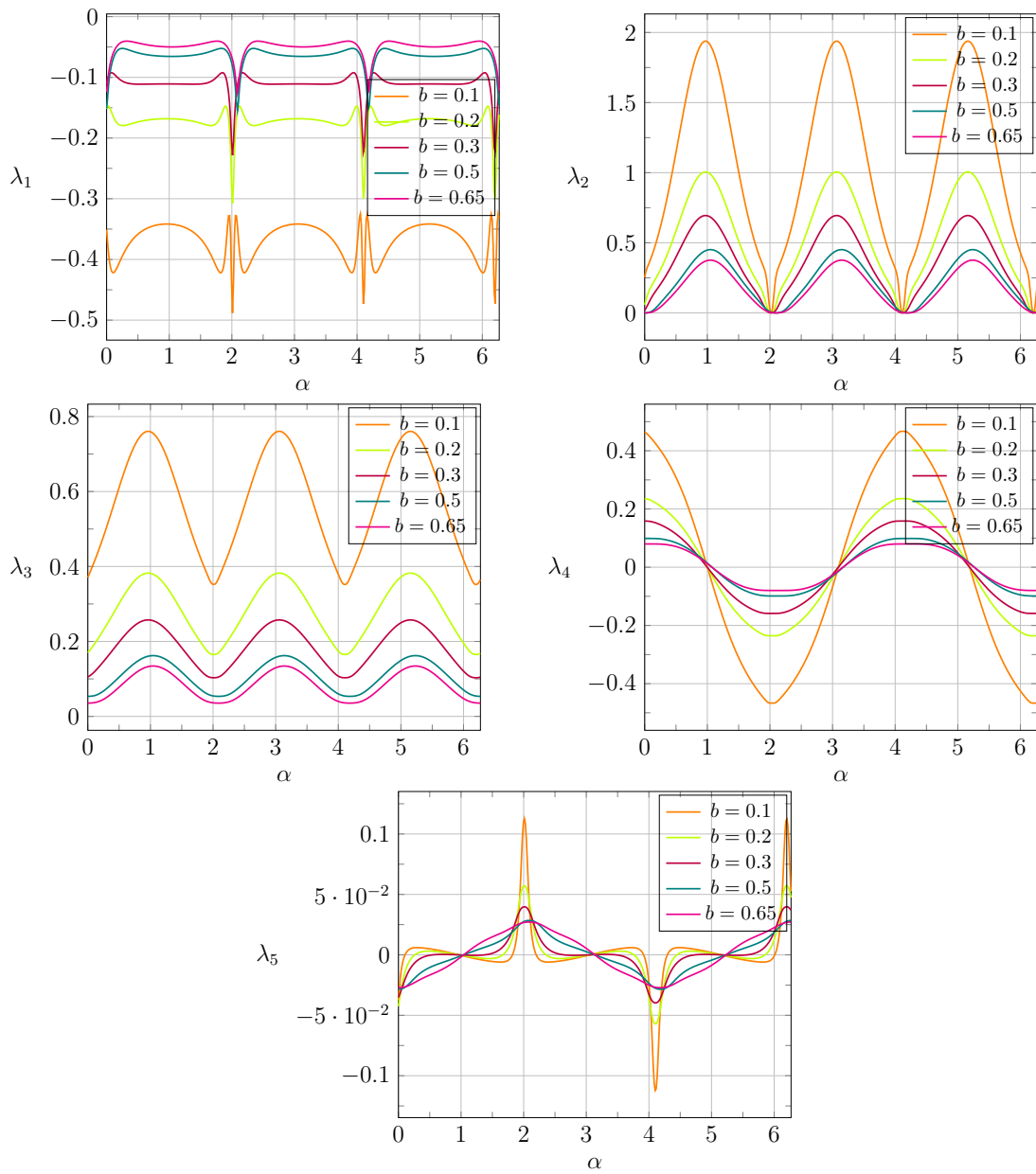


Figure 3.13: Lagrange multipliers of the  $3\pi$ -twisted Möbius bands.

$N \in \{20, 40, 80, 160\}$  and look at the behavior of the eigenvalues of the projected Hessian (2.58). We use this configuration as we do not have doubt that its continuous counterpart is at least a local minimum of the corresponding continuous problem. We sort, equidistantly distribute on the interval  $[0, 1]$ , and plot the eigenvalues as in Figure 3.14 (left plot). We employ a logarithmic scale to demonstrate the arising issue. As we can see from the figure, approximately half of the multipliers of the left-hand side are of similar magnitude for each value of  $N$ . As  $N$  increases, the magnitude decreases and goes to zero. Thus, we conjecture that the behaviour of the energy functional near critical points might be of order higher than two and thus that stability cannot be checked by the second variation condition. Similar behavior is also observed for the Möbius bands (right plot in Figure 3.14). Hence, we cannot make definite statements about the stability of the continuous counterpart of the obtained solutions. Additionally, these small eigenvalues affect numerical convergence to the discrete solution.

### 3.6 Energy convergence for $\pi$ -twisted bands

In Chapter 2 we have shown some *a priori* results for convergence of the discrete augmented energy functional to the continuous one. In this section we provide some *a posteriori* results that support the theoretical calculations for  $\pi$ -twisted bands. As we do not know the exact solution, we access the convergency rate on a sequence of grids. For this we define the quantity

$$\Delta_N = |E_N - E_{2N}|, \quad (3.11)$$

where  $E_N$  is the discrete energy of the discrete band with  $N$  flat elements. From Table 3.1, we can see that for all of the aspect ratios the convergency rate is better or as the theoretically computed one in Chapter 2.

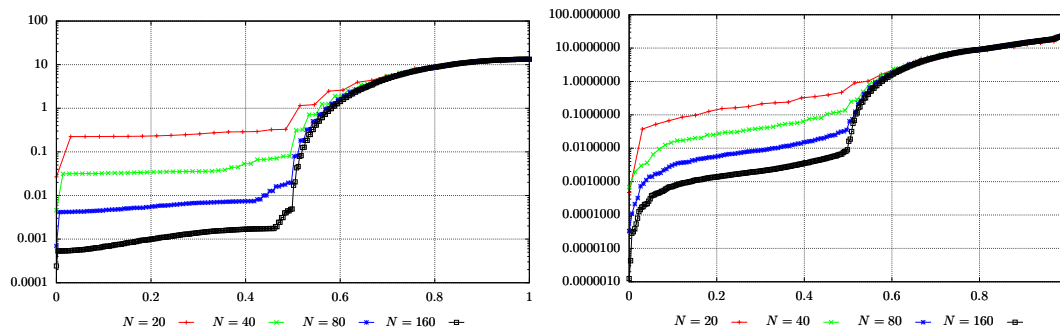


**Figure 3.14:** Sorted and equally distributed on  $[0, 1]$  eigenvalues of the projected Hessian in a logarithmic scale. The left plot corresponds to a cylindrical band of length  $\ell = 2\pi$  and half-width  $b = 0.3$ , and the right plot corresponds to a  $\pi$ -twisted Möbius band of length  $\ell = 2\pi$  and half-width  $b = 0.5$

half-width	N	$\Delta_N$	$\Delta_N/\Delta_{2N}$	$\log_2(\Delta_N/\Delta_{2N})$
$b = 0.1$	50	0.0419388	102.457	6.679
	100	0.000409329	16.7572	4.067
	200	$2.4427e^{-5}$	-	-
$b = 0.2$	50	0.00425294	5.88271	2.5565
	100	0.000722955	5.85097	2.5487
	200	0.000123562	-	-
$b = 0.5$	50	0.0124391	4.38177	2.1315
	100	0.00283882	4.16469	2.0582
	200	0.00068164	-	-
$b = 0.8$	50	0.0303446	4.13269	2.047
	100	0.00734258	4.04805	2.0172
	200	0.00181386	-	-
$b = 1.0$	50	0.0594413	4.08444	2.03
	100	0.0145531	4.02676	2.0096
	200	0.0036141	-	-
$b = 1.5$	50	1.90428	5.80436	2.537
	100	0.328078	4.29908	2.104
	200	0.0763136	-	-

**Table 3.1:** Energy convergence results for various half-width of the  $\pi$ -twisted bands



# Conclusions

In this section, we summarize what is done in the thesis and propose possible future directions of the study. We first mention the main results of the present thesis as bullet points.

- We considered an injective isometric deformation of a two-dimensional homogeneous and isotropic solid identified with a right-circular cylindrical reference configuration  $\mathcal{D}$  into a band that occupies the surface  $\mathcal{S}$  in three-dimensional Euclidean point space and derived the necessary and sufficient conditions for the deformation to be isometric.
- We also performed dimensional reduction of the bending energy for the deformation above.
- As the energy functional has significant singularities that complicate the development of a numerical approach, we introduce an additional variable that removes the singularity. Also, this change allows us to consider an optimization problem that only has equality constraints.
- For the new formulation of the problem we derived the Euler-Lagrange equations and explicitly calculated the Lagrange multipliers in terms of the directrix and generatrix.
- We discretized the continuous model and showed how to reconstruct a continuous surface from a solution to the discrete optimization problem. The continuous surface is reconstructed so that the corresponding continuous energy functional is approximated by the discrete one in the second order of  $h$ .
- To solve the discrete optimization problem numerically, we developed a saddle-free Newton method for constrained optimization.
- Finally, we provided the first attempt to find the partially everted cylinder and numerical solutions for  $\pi$  and  $3\pi$  twisted Möbius bands. We also performed the stability analysis for all of the discrete solutions.

There are several intriguing questions that we can foresee for future research. We write them down as bullet points below.

- We could not find a way to obtain the discrete partially everted cylinder for refined discretization and wider range of aspect ratios. Thus, we did not answer the question of the existence of the partially everted cylinder. Also, the critical

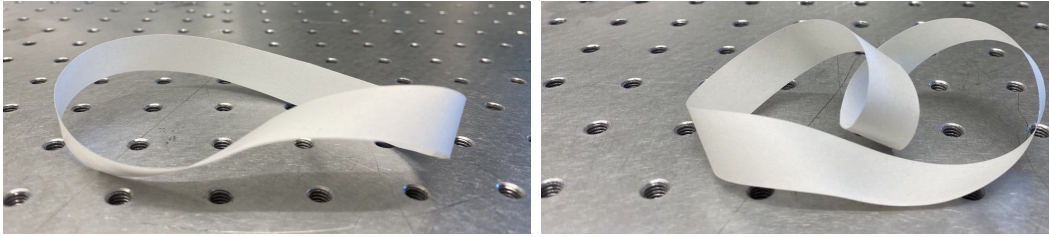


**Figure 3.15:** Möbius band made of a paper strip and a partially everted Möbius band obtained from it by an isometric deformation.

maximum and, probably, minimum aspect ratio of the partially everted cylinder is to be studied if the partially everted cylinder exists.

- We also think that it is vital to solve the vanishing eigenvalue problem and to figure out how we can check the stability of the continuous model.
- There is a possibility of having a  $\pi$ -twisted Möbius band different from the conventional shape 3.15. We call this partially everted Möbius band and it is intriguing to figure out if such configuration is stable or not.

This thesis provides a robust algorithm for computing equilibrium shapes for unstretchable elastic ribbons. The new bilateral injectivity constraint makes it possible to compute some shapes (at least the  $3\pi$ -twisted Möbius band) for wider range of aspect ratios than it was done before. Additionally, the Saddle-free Newton method developed in 2 can be applied to any finite dimensional optimization problem with bilateral constraints. With some additional modification (eg active set method [18]), it can also be applied to wider range of optimization problems with bilateral and unilateral constraints.

# Bibliography

- [1] J. Schönke, M. Grunwald, and E. Fried, *Construction of Unknotted and Knotted Symmetric Developable Bands*, *Symmetry* **13** (2021).
- [2] L. Koens and E. Lauga, *Slender-ribbon theory*, *Physics of Fluids* **28**, 013101 (2016).
- [3] Y. Forterre and J. Dumais, *Generating Helices in Nature*, *Science* **333**, 1715–1716 (2011).
- [4] J. Lighthill and R. Blake, *Biofluidynamics of balistiform and gymnotiform locomotion. Part 1. Biological background, and analysis by elongated-body theory*, *Journal of Fluid Mechanics* **212**, 183–207 (1990).
- [5] A. A. Shirgaonkar, O. M. Curet, N. A. Patankar, and M. A. MacIver, *The hydrodynamics of ribbon-fin propulsion during impulsive motion*, *Journal of Experimental Biology* **211**, 3490–3503 (2008).
- [6] D. C. Richardson and J. S. Richardson, *Teaching molecular 3-D literacy*, *Biochemistry and Molecular Biology Education* **30**, 21–26 (2002).
- [7] S. Tanda, T. Tsuneta, Y. Okajima, K. Inagaki, K. Yamaya, and N. Hatakenaka, *A Möbius strip of single crystals*, *Nature* **417**, 397–398 (2002).
- [8] J. Gravesen and M. Willatzen, *Eigenstates of Möbius nanostructures including curvature effects*, *Phys. Rev. A* **72**, 032108 (2005).
- [9] M. Sadowsky, *Ein elementarer Beweis für die Existenz eines abwickelbaren Möbiusschen Bandes und die Zurückführung des geometrischen Problems auf ein Variationsproblem.*, *Sitzungsberichte der Preussischen Akademie der Wissenschaften, physikalisch-mathematische Klasse* **22**, 412–415 (1930).
- [10] D. F. Hinz and E. Fried, *Translation of Michael Sadowsky’s Paper “An Elementary Proof for the Existence of a Developable Möbius Band and the Attribution of the Geometric Problem to a Variational Problem*, *Journal of Elasticity* **119**, 3–6 (2015).
- [11] W. Wunderlich, *Über ein abwickelbares Möbiusband*, *Monatshefte für Mathematik* **66**, 276–289 (1962).
- [12] R. E. Todres, *Translation of W. Wunderlich’s “On a Developable Möbius Band”*, *Journal of Elasticity* **119**, 23–34 (2015).

- 
- [13] E. L. Starostin and G. H. M. van der Heijden, *The shape of a Möbius strip*, Nature Materials **6**, 563–567 (2007).
- [14] E. L. Starostin and G. H. M. van der Heijden, *Equilibrium Shapes with Stress Localisation for Inextensible Elastic Möbius and Other Strips*, Journal of Elasticity **119**, 67–112 (2015).
- [15] A. Moore and T. Healey, *Computation of elastic equilibria of complete Möbius bands and their stability*, Mathematics and Mechanics of Solids **24**, 939–967 (2019).
- [16] Y.-C. Chen, R. Fosdick, and E. Fried, *Isometric deformations of unstretchable material surfaces, a spatial variational treatment*, Journal of the Mechanics and Physics of Solids **116**, 290–322 (2018).
- [17] B. Seguin, Y.-c. Chen, and E. Fried, *Closed unstretchable knotless ribbons and the Wunderlich functional*, Journal of Nonlinear Science, 2577–2611 (2020).
- [18] J. Nocedal and S. Wright, *Numerical Optimization*, Springer New York (2000).
- [19] P. Hornung, *Euler-lagrange equation and regularity for flat minimizers of the Willmore functional*, Communications on Pure and Applied Mathematics **64**, 367–441 (2011).
- [20] Y. N. Dauphin, R. Pascanu, C. Gulcehre, K. Cho, S. Ganguli, and Y. Bengio. *Identifying and Attacking the Saddle Point Problem in High-Dimensional Non-Convex Optimization*. In *Proceedings of the 27th International Conference on Neural Information Processing Systems - Volume 2*, pages 2933–2941, Cambridge, MA, USA, (2014). MIT Press.
- [21] L. Mahadevan and J. B. Keller, *The shape of a Möbius band*, Proceedings of the Royal Society of London. Series A: Mathematical and Physical Sciences **440**, 149–162 (1993).
- [22] Y.-c. Chen, R. Fosdick, and E. Fried, *Issues concerning isometric deformations of planar regions to curved surfaces*, Journal of Elasticity **132**, 1–42 (2018).
- [23] J. J. Callahan, *Advanced Calculus* (2010).